UNIVERSITY OF MINNESOTA

ST. ANTHONY FALLS LABORATORY

Engineering, Environmental and Geophysical Fluid Dynamics

Project Report No. 605

Measuring the Effectiveness of Submersed Jets to Minimize Invasive Species Transport

by

Andrew J. Erickson and William R. Herb

St. Anthony Falls Laboratory, University of Minnesota

Prepared for

Hennepin County

November 2023

Minneapolis, Minnesota

Cite as: Erickson, A.J., W.R. Herb (2023). "Measuring the Effectiveness of Submersed Jets to Minimize Invasive Species Transport." Project Report No. 605, St. Anthony Falls Laboratory, University of Minnesota, Minneapolis, MN. November 2023.

The University of Minnesota shall provide equal access to and opportunity in its programs, facilities, and employment without regard to race, color, creed, religion, national origin, gender, age, marital status, disability, public assistance status, veteran status, sexual orientation, gender identity, or gender expression.

Any opinions, findings, conclusions, or recommendations expressed in this publication are those of the original author(s) and do not necessarily reflect the view of the Compost Research and Education Foundation or the University of Minnesota.

ACKNOWLEDGEMENTS

This project was supported financially by Hennepin County. The authors are grateful to Tony Brough, the Aquatic Invasive Species (AIS) prevention program coordinator, for his diligence and insights throughout the project. The authors thank administrative staff at both Hennepin County and the University of Minnesota (U of M) for securing the contract and handling the transfer of funds. The authors thank Hennepin County Sheriff and Water Patrol staff for allowing us access to their boat launch for some of our measurements.

TABLE OF CONTENTS

Acknowledgements....3
Table of Contents....4
Table of Figures....4
1 Introduction....7
2 Field Vegetation Measurements....7
2.1 Site: Spring Park Water Patrol....8
2.2 Site: Spring Park Public Access....11
2.3 Site: Weaver Lake Public Access....12
2.4 Field Vegetation Measurements Summary and Conclusions....13
3 Field ADV Measurements....14
4 Conclusions and Recommendation....20
5 Drone data availability....21
6 Supplemental Information – Verification of Simulations....21
6.1 Computer Simulations & Lab Verification....21
6.1.1 Estimating jet velocities....21
6.1.2 Laboratory testing of an Aqua Thruster....23
6.1.3 CFD Models for Turbulent Jets in Deep and Shallow Water....25
6.1.4 CFD model for the Aqua Thruster in the SAFL Main Channel....26
6.1.5 CFD model for the Aqua Thruster in a wide channel....29
7 References....32

TABLE OF FIGURES

Figure 1: Suspended Plant Fragment Collection at Water Patrol Boat Ramp, six feet from shore. 8
Figure 2: Overview map of Spring Park Boat Ramps on Lake Minnetonka (image courtesy Google Earth). 8
Figure 3: Approximate Location of Vegetation Fragment Collection Transects at Spring Park Water Patrol Boat Ramp (image courtesy Google Earth). 9
Figure 4: Dry weight of suspended vegetation fragments at the Spring Park Water Patrol boat ramp with (orange bars) and without (green bars) the submersed jet in operation. 9
Figure 5: Accumulated vegetation fragments near the submersed jet at Spring Park Water Patrol (jet marked with red buoy; turbulence from jet evident on the surface). 10
Figure 6: Accumulated vegetation fragments near the submersed jet at Spring Park Public Access (jet located under the dock; turbulence from jet evident on the surface) (image courtesy Bolton & Menk). ..10
Figure 7: Approximate Location of Vegetation Fragment Collection Transects at Spring Park Public Access (image courtesy Google Earth)....11

Figure 8: Dry weight of suspended vegetation fragments at the Spring Park Public Access boat ramp with (orange bars) and without (green bars) the submersed jet in operation. 12
Figure 9: Approximate Location of Vegetation Fragment Collection Transects at Weaver Lake Public Access (image courtesy Google Earth). 12
Figure 10: Dry weight of suspended vegetation fragments at the Weaver Lake Public Access boat ramp with (orange bars) and without (green bars) the submersed jet in operation. 13
Figure 11: Point cloud of 32 surveyed locations in which ADV measurements were collected, and a contour plot of the surface velocities at Spring Park Public Access. 14
Figure 12: Point cloud of 23 surveyed locations in which ADV measurements were collected, and a contour plot of the surface velocities at Spring Park Water Patrol. 15
Figure 13: Example of 45-second velocity measurements at the public access boat ramp (Note 1 m/s = 3.28 ft/s). Vx is the velocity in the x-direction, approximately pointed towards the jet source, Vy is the lateral velocity, as shown above. The velocity magnitude is then $\boldsymbol{Vmag = Vx2 + Vy2}$ 16
Figure 14: Velocity magnitude contours at the public boat ramp for measurements 6 inches below water surface (upper panel) and mid-depth (lower panel). Note: 10m = 32.8ft; 70m = 230ft; 0.2 m/s = 0.66 ft/s 17
Figure 15: Velocity magnitude contours at the Sheriff's boat ramp for measurements 6 inches below water surface (upper panel) and mid-depth (lower panel). Note: 10m = 32.8ft; 90m = 295ft; 0.5 m/s = 1.64 ft/s 18
Figure 16: Scatter plot of all measured velocity magnitudes vs. distance from jet source for the public ramp (upper panel) and the Sheriff's ramp (lower panel). Also shown are fits to the maximum velocity magnitude vs. distance (r). Note 1 m/s = 3.28 ft/s; 80m = 260ft 19
Figure 17: Propeller exit velocity vs. motor horsepower for a 7 in. diameter propeller, based on Equation 1. 21
Figure 18: Schematic diagram of a submerged jet produced by a motor and propeller. 22
Figure 19: Estimated jet centerline velocity and jet diameter over distance, from Equation 2. The width is based on the distance from the jet centerline where the velocity is 37% of the centerline velocity. 22
Figure 20: Map view of the experimental setup of the Aqua Thruster in the SAFL main channel (not to scale). 23
Figure 21: Photographs of the Aqua Thruster installed in the SAFL main channel (left) and the surface jet produced by the Aqua Thruster and the ADV used to measure velocities suspended from the data carriage (right). 24
Figure 22: Velocity magnitude vs. distance (x-direction) along the channel center (y=0) and at a depth of 10 cm (3.9 in). 24
Figure 23: Schematic of the CFD model domain for modeling the decay of a turbulent round jet. 25
Figure 24: Plot of modeled velocity magnitude along the domain centerline, near the jet source, for the 2 m thick domain and a 15 cm diameter jet at the inlet. 25
Figure 25: Simulated decay rate of centerline jet velocity for 40 m, 10 m, and 2 m thick domains, along with the free jet solution (Eq. 2) and a line with slope $x^{-1/4}$. 2 m FS has a frictionless surface on the top of the domain. 26
Figure 26: Detail schematic of the representation of the Aqua Thruster in the CFD model. 26
Figure 27: Plot of modeled velocity magnitude near the Aqua Thruster along the channel and jet center line (y=0) for the motor set at a 10° angle from horizontal. 27
Figure 28: Plot of modeled velocity (x-component) near the Aqua Thruster at the water surface for the motor set at a 10° angle from horizontal. Note that the velocity is negative near the edges due to recirculating flow. 27

Figure 29: Plot of observed and modeled (CFD) velocity magnitude vs. distance (x-direction) along the jet center line. Modeled velocities are given for 4 different motor angles from horizontal. 28
Figure 30: Plot of observed and modeled (CFD) velocity magnitude vs. lateral distance (y-direction) at 1 m and 4 m downstream from the Aqua Thruster. Modeled velocities are given for a 20° angle from horizontal. 28
Figure 31: Plot of observed and modeled (CFD) velocity magnitude vs. vertical distance (z-direction) at 1 m downstream from the Aqua Thruster. Modeled velocities are given for the motor at a 20° angle from horizontal. 29
Figure 32: Contour plots of surface velocity magnitude (upper panel) and bottom shear stress (lower panel) for the motor at a 15° angle from horizontal. 30
Figure 33: Velocity vs. distance at the water surface above the jet centerline for motor angles of 9°, 10°, 15°, and 20° from horizontal. A line that follows x^-1/4 is also given for reference. 31
Figure 34: Velocity vs. distance at the water surface above the jet centerline for 1 m and 2 m deep channels and a 10° motor angle. 32
Figure 35: Simulated maximum bed shear stress vs. motor angle for a 1 m deep channel. 32

1 Introduction

Preventing the spread of aquatic invasive species (AIS) is of paramount importance for the protection of Minnesota's water resources. Staff from the University of Minnesota (U of M) St. Anthony Falls Laboratory (SAFL) worked in coordination with Hennepin County AIS prevention staff to investigate the ability of submersed jets to minimize floating and suspended vegetation fragments near and on boat launch ramps. As boats are loaded onto trailers, floating and suspended plant fragments can become trapped between the boat and the trailer pads. Trapped fragments are challenging or impossible to remove at AIS removal stations because the weight on the boat holds them in place. In addition, trailers pads often have a carpet or fabric non-slip covering, creating small crevices into which plant fragments can become trapped and challenging to remove. When the boat is redeployed elsewhere, however, these plant fragments can be released as the boat enters the water and the trailer pads become submerged. AIS can be spread to waterbodies throughout Minnesota if these plant fragments are, or contain, AIS.

The objective of this project was to measure the effectiveness of submersed jets to minimize the transport of aquatic invasive species (AIS) near boat ramps within Hennepin County. The hypothesis is that submersed jets push suspended plant fragments away from the boat ramps while boats are trailered, thus reducing the potential for plant fragments to become trapped on boat trailer pads and transported to other waterbodies. The first activity was to measure how much suspended vegetation was in the vicinity of the boat ramp with and without the jet in operation. A net was used to capture suspended vegetation in the area around the boat ramp. The second activity was to measure the velocity in the lake within the area of effect created by the jet at the Spring Park Boat Ramps. The purpose of these measurements was to compare real field velocity measurements to the computer simulations to improve the recommendations of submersed jet operation.

2 Field Vegetation Measurements

Three boat ramps were selected for field measurements: Spring Park Water Patrol access, Spring Park Public Access, and Weaver Lake Public Access. At each site, a submersed jet was installed, connected to a power source, and aimed slightly above level and towards the water surface (vertical direction). For the Spring Park ramps, the jet was aimed approximately parallel with the shore but at an angle towards the boat ramp and shore (horizontal direction). For Weaver Lake, the jet was located under the public access dock and aimed towards the lake at approximately a 45° angle from parallel to the shore, and away from the ramp.

During a field test, a telescoping mesh net was pushed through the water from the surface to a depth of approximately 30 cm (12 inches) below the water surface in a transect parallel to the shore to capture suspended vegetation fragments (see Figure 1). The net was passed over the transect three times. Vegetation samples were collected before the jet was turned on, while the jet was running, and sometimes after the jet was turned off. Vegetation captured by the net was put into Ziplock bags, labeled, and sealed to preserve moisture and vegetation. For analysis, the samples were dewatered with a salad spinner and placed into heat-resistant metal trays and dried at 96°C (205°F) for at least 24 hours or until the sample weight did not change. The dry weight was recorded and used for data analysis.

Figure 1: Suspended Plant Fragment Collection at Water Patrol Boat Ramp, six feet from shore.

2.1 Site: Spring Park Water Patrol

The Spring Park Water Patrol boat ramp is a single vehicle-width ramp controlled by the Hennepin County Sheriff's Office, located on Lake Minnetonka near 4141 Shoreline Dr. Spring Park, MN 55384 (see Figure 2). For vegetation measurements, two transects parallel to the shoreline were traversed to collect suspended vegetation fragments (see Figure 3). The vegetation samples were collected on September 2, 2022 at approximately 9am, and the transects were approximately five feet and ten feet into the lake from the southernmost point of the seawall, respectively.

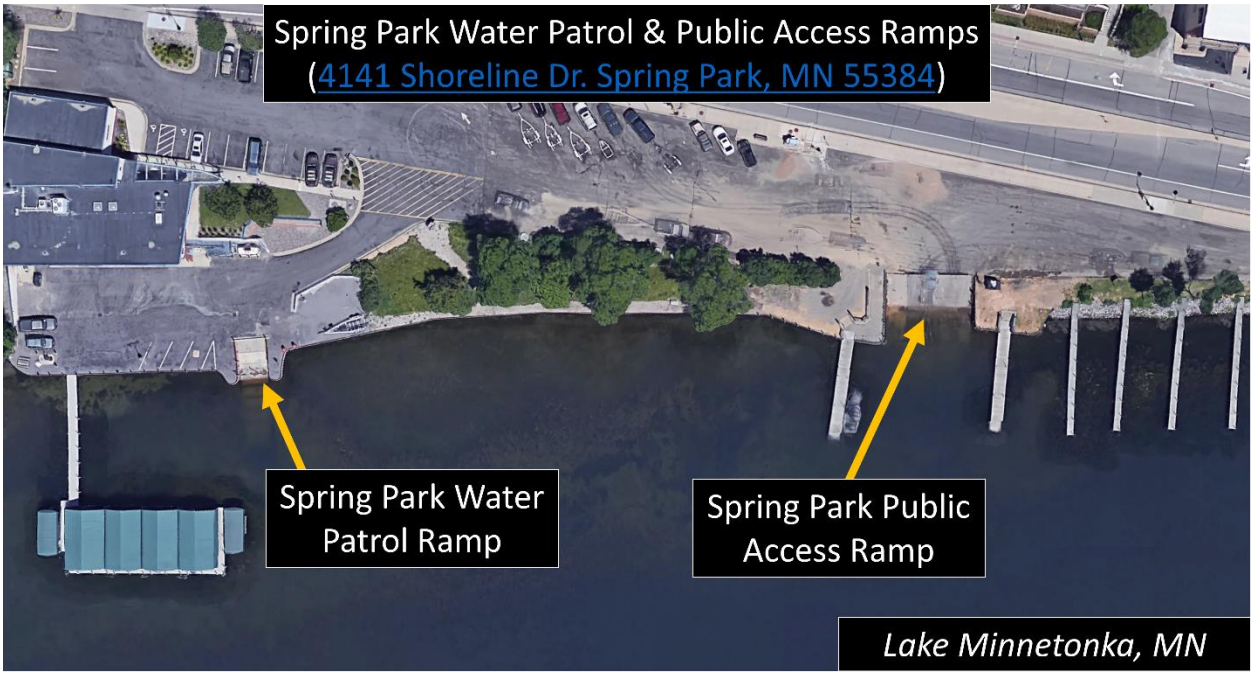

Figure 2: Overview map of Spring Park Boat Ramps on Lake Minnetonka (image courtesy Google Earth).

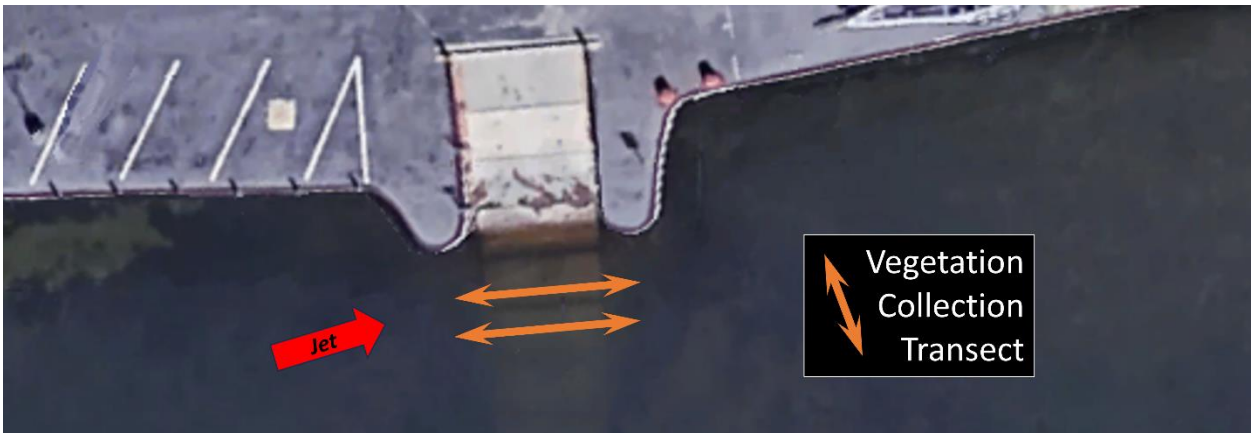

Figure 3: Approximate Location of Vegetation Fragment Collection Transects at Spring Park Water Patrol Boat Ramp (image courtesy Google Earth).

The suspended vegetation collection results are shown in Figure 4. For the near shore measurements (5 ft), both samples before and after the jet was in operation produced a larger mass of suspended vegetation fragments compared to the sample collected when the jet was in operation (Figure 4). This suggests that less suspended vegetation fragments were present at this distance from the shore when the submerged jet was operating compared to when the jet was not operating. In other words, it appears the submersed jet reduced the amount of suspended vegetation in the vicinity of the boat ramp at five feet from the shore at the Water Patrol boat ramp.

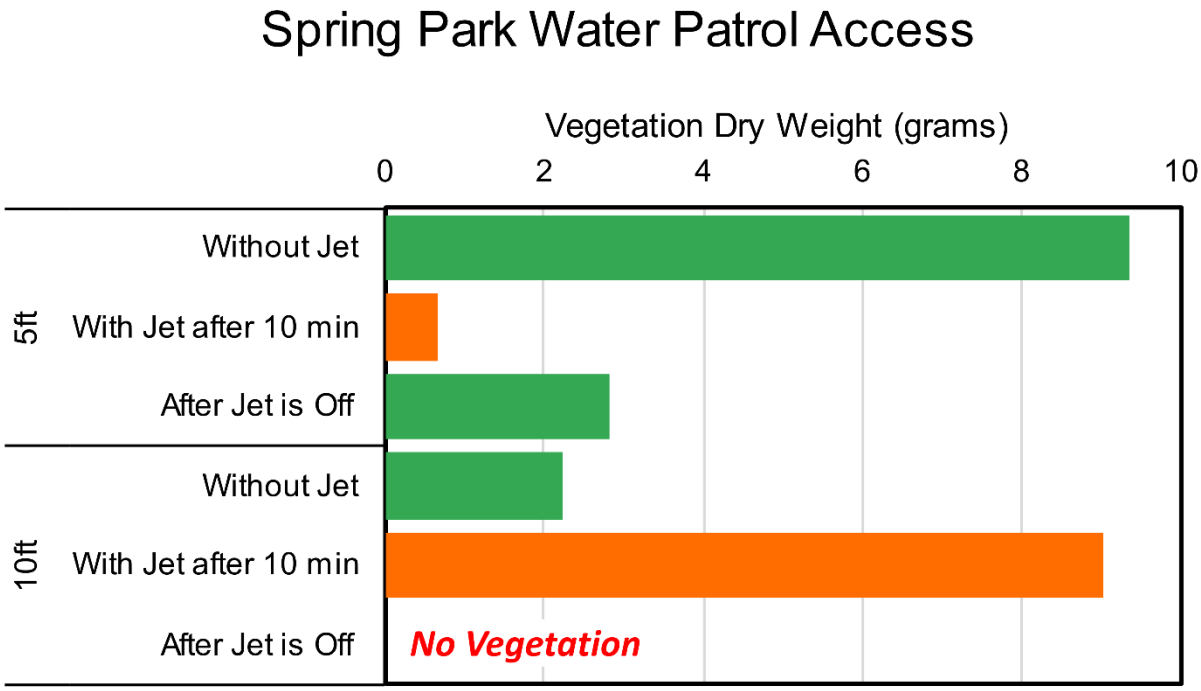

Figure 4: Dry weight of suspended vegetation fragments at the Spring Park Water Patrol boat ramp with (orange bars) and without (green bars) the submersed jet in operation.

In contrast, the presence of suspended vegetation at approximately 10ft from the shore was greater when the jet was in operation compared to when the jet was not operating (Figure 4). Recirculation zones and accumulation of suspended vegetation fragments were observed near the edges of the area of

effect caused by the jet. Sometimes, the jet also pulled suspended vegetation from behind the jet or along the seawall and pushed it towards the boat ramp (see Figure 5 and Figure 6). This increased the vegetation fragments in the vicinity of the boat ramp if there was accumulation of vegetation behind or near the jet. After the jet was turned off, however, no vegetation mass was captured in the net (Figure 4). This suggests that the jet was successful in reducing vegetation in the vicinity of the boat ramp but may have been impacted by a mass of vegetation behind the jet while the jet was operating.

Figure 5: Accumulated vegetation fragments near the submersed jet at Spring Park Water Patrol (jet marked with red buoy; turbulence from jet evident on the surface).

Figure 6: Accumulated vegetation fragments near the submersed jet at Spring Park Public Access (jet located under the dock; turbulence from jet evident on the surface) (image courtesy Bolton & Menk).

2.2 Site: Spring Park Public Access

The Spring Park Public Access boat ramp is approximately the width of three vehicles, located on Lake Minnetonka near 4141 Shoreline Dr. Spring Park, MN 55384 (see Figure 2). For vegetation measurements, two transects parallel to the shoreline were traversed to collect suspended vegetation fragments (see Figure 7). The vegetation samples were collected on September 2, 2022, at approximately 10am, and the transects were approximately 0 feet and 6 feet into the lake from the southernmost point of the seawall (west of the ramp), which was 12 ft and 18 ft from the waterline, respectively.

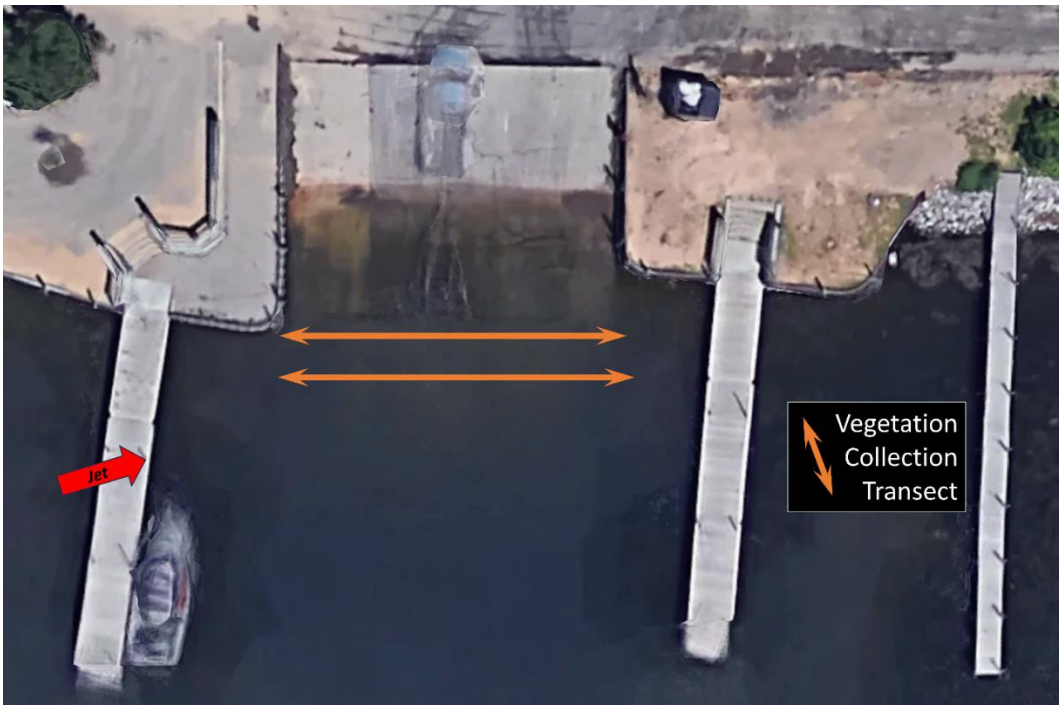

Figure 7: Approximate Location of Vegetation Fragment Collection Transects at Spring Park Public Access (image courtesy Google Earth).

The suspended vegetation collection results are shown in Figure 8. For the near shore measurements (12 ft), the mass of vegetation before the jet was in operation was the largest mass of all samples. Both samples collected while the jet was in operation (15 min and 30 min of operation) produced less vegetation compared to before the jet was operating. This suggests that the jet reduced the amount of suspended vegetation fragments in the water in the vicinity of the boat ramp 12 ft away from shore. The mass of vegetation after the jet was turned off was less than when the jet was operating and before the jet was operating. This suggests that the jet's ability to reduce suspended vegetation fragments persists for a short period of time (5 – 10 min) after the jet is turned off.

Farther from shore (18 ft), the mass of suspended vegetation fragments was largest before the jet was turned on and less during and after the jet was in operation (Figure 8). This is consistent with the observation at 12 ft from shore; that the jet reduced the amount of suspended vegetation fragments in the water in the vicinity of the boat ramp 18ft away from shore.

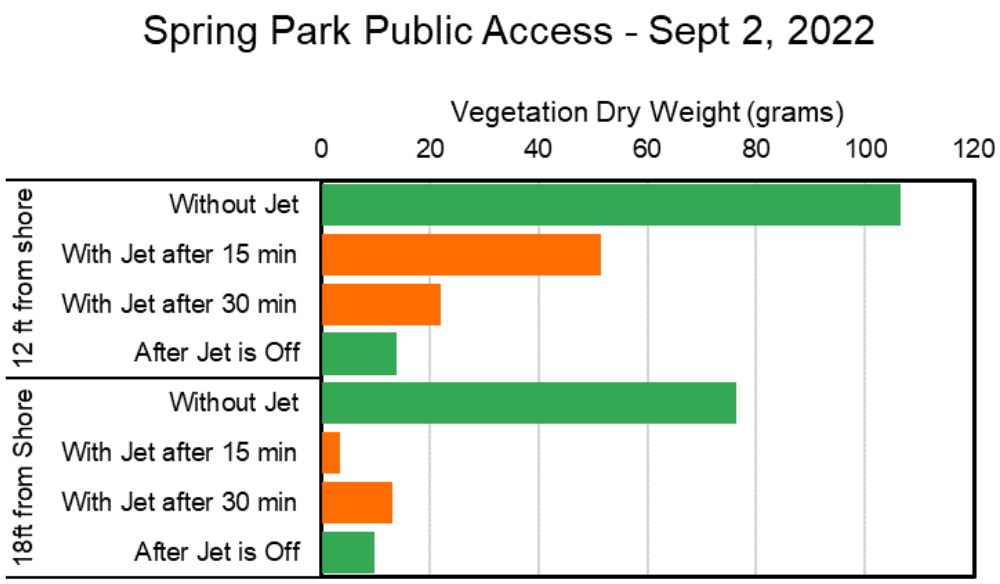

Figure 8: Dry weight of suspended vegetation fragments at the Spring Park Public Access boat ramp with (orange bars) and without (green bars) the submersed jet in operation.

2.3 Site: Weaver Lake Public Access

The Weaver Lake Public Access boat ramp is a single vehicle width boat ramp located on Weaver Lake, near 18281 Weaver Lake Dr, Osseo, MN 55311 (see Figure 9). For vegetation measurements, two transects parallel to the shoreline were traversed to collect suspended vegetation fragments (see Figure 9). The vegetation samples were collected on September 8, 2022 at approximately 9:30am, and the transects were approximately 0 feet and 8 feet into the lake from the easternmost point of the public access dock, which was 12ft and 20ft from the waterline, respectively.

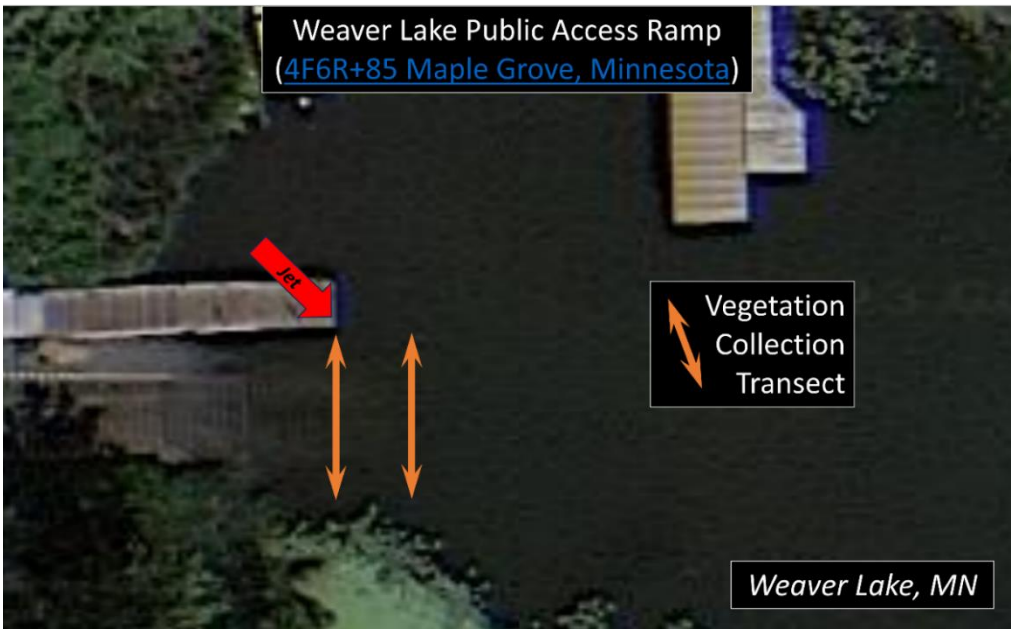

Figure 9: Approximate Location of Vegetation Fragment Collection Transects at Weaver Lake Public Access (image courtesy Google Earth).

The suspended vegetation collection results are shown in Figure 10. For the near shore measurements (12 ft), the mass of vegetation before the jet was in operation was less than the mass collected after the jet was operating. This could be due to vegetation fragments accumulated under the dock where the submersed jet was located. Before operation, the natural background suspended vegetation fragments (i.e., without jet operation) were present in the vicinity of the boat ramp. When the jet was turned on, it may have mobilized vegetation that had accumulated under the dock, which was captured in the net during sampling. The jet was aligned facing into the lake, which creates a recirculation zone between the centerline of the jet and the shore, immediately over the ramp itself. The near shore (12 ft) transect passes directly through this recirculation zone, which could explain why more vegetation was collected while the jet was running.

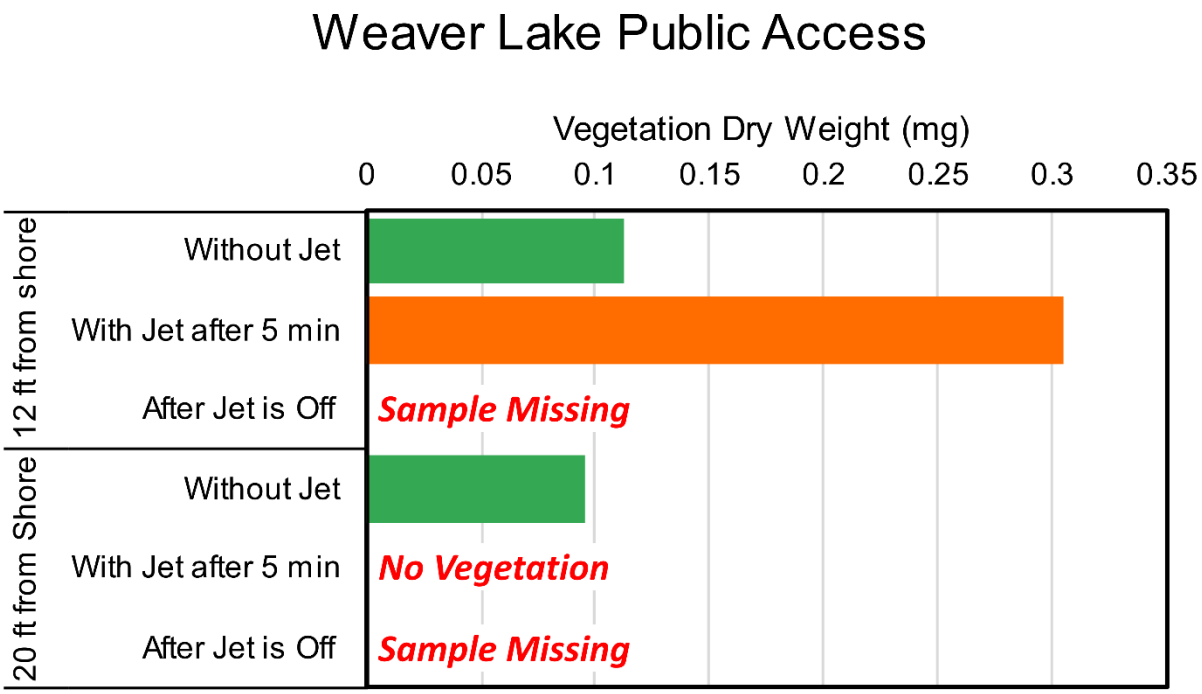

Figure 10: Dry weight of suspended vegetation fragments at the Weaver Lake Public Access boat ramp with (orange bars) and without (green bars) the submersed jet in operation.

Further from shore (20 ft), the suspended vegetation fragments collected before the jet was in operation was similar to the mass collected near shore (12 ft, see Figure 10), which confirms the natural background suspended vegetation mass near the boat ramp. At 20 ft from shore, the mass collected while the jet was operating was less than before the jet was turned on, suggesting the jet reduced the amount of suspended vegetation fragments in the water in the vicinity of the boat ramp 20 ft away from shore. The jet was allowed to operate for a total of ten minutes before it was turned off and samples were collected (after jet is off). These post-jet-operation samples, however, were lost between collection and sample analysis, and thus no data is available.

2.4 Field Vegetation Measurements Summary and Conclusions

In general, most (67%) observations showed less mass of suspended vegetation fragments with the jet operating compared to the mass of suspended vegetation fragments before the jet was turned on. For the rest of the tests (33%), more suspended vegetation fragments were present with the jet operating. For the 33% of tests in which vegetation fragments increased, there were suspended plant fragments

near the jet when it was turned on, which caused an increase in transport of the plant fragments towards the jet. To overcome this challenge, 1) the jet should be placed away from areas where plant fragments will accumulate, 2) plant fragment accumulation should be prevented around and near the jet, or 3) accumulated plant fragments should be prevented from being pulled in by the submersed jets and pushed out towards the boat ramps. In some tests, the amount of suspended plant fragments after the jet was turned off was less than before the jet was turned on, indicating that the jet provided a positive effect for some time after operation. This post-operation effect was not measured, but visual observations suggested the benefit would last until natural wind-driven transport of suspended plant fragments pushed fragments back into the area of the jet's influent.

3 Field ADV Measurements

Acoustic Doppler Velocimeter (ADV) field measurements were taken at the Spring Park Public Access boat ramp and the Water Patrol boat ramp at the Spring Park Bay of Lake Minnetonka, MN. A 2D Sontek field ADV was used to measure water velocity and a Total Station was used to measure the location of each velocity measurement in the lake. Several transects were selected perpendicular to the centerline of the jet's cone-shaped area of effect. At each location, the water depth was measured, and velocity measured at one to three different depths: typically one measurement 6 inches below the water surface and a second measurement at mid-depth. If the water depth was greater than ~24 inches, then three measurements were collected: 6 inches below the water surface, 6 inches above the lake bottom, and mid-depth. The Public Access had 32 locations that were surveyed and measured on August 24, 2023 (see Figure 11), and the Sheriff's boat ramp had 23 locations that were surveyed and measured on September 6, 2023 (see Figure 12).

Figure 11: Point cloud of 32 surveyed locations in which ADV measurements were collected, and a contour plot of the surface velocities at Spring Park Public Access.

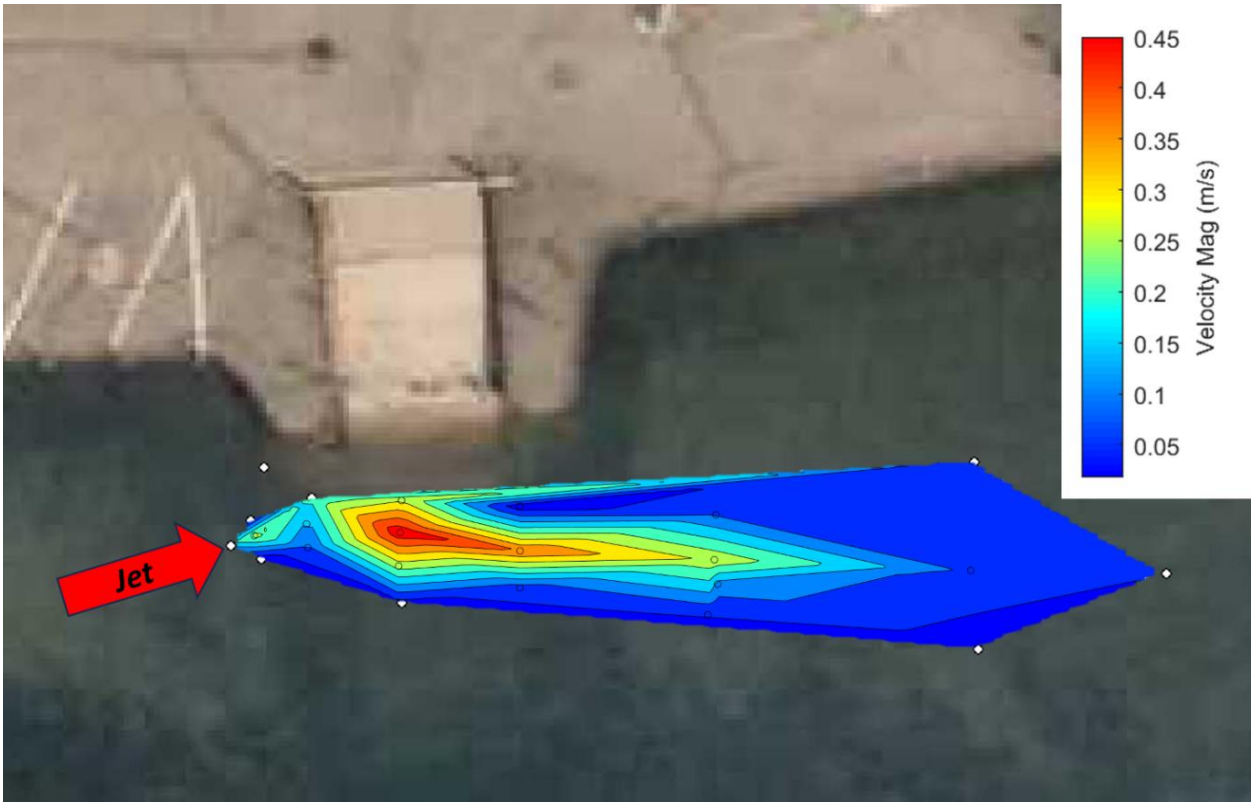

Figure 12: Point cloud of 23 surveyed locations in which ADV measurements were collected, and a contour plot of the surface velocities at Spring Park Water Patrol.

Each velocity measurement using the field ADV was taken over 45 seconds at a 1 Hz sampling rate and is reported as the average velocity magnitude over the 45 second duration. However, the measured velocities were typically quite turbulent, with velocity fluctuations similar in magnitude to the mean velocity (Figure 13). In addition to the measurements described above with the submersed jet turned on, several water velocity measurements were taken with the jet turned off, and several landmarks around the boat ramps were surveyed as reference points.

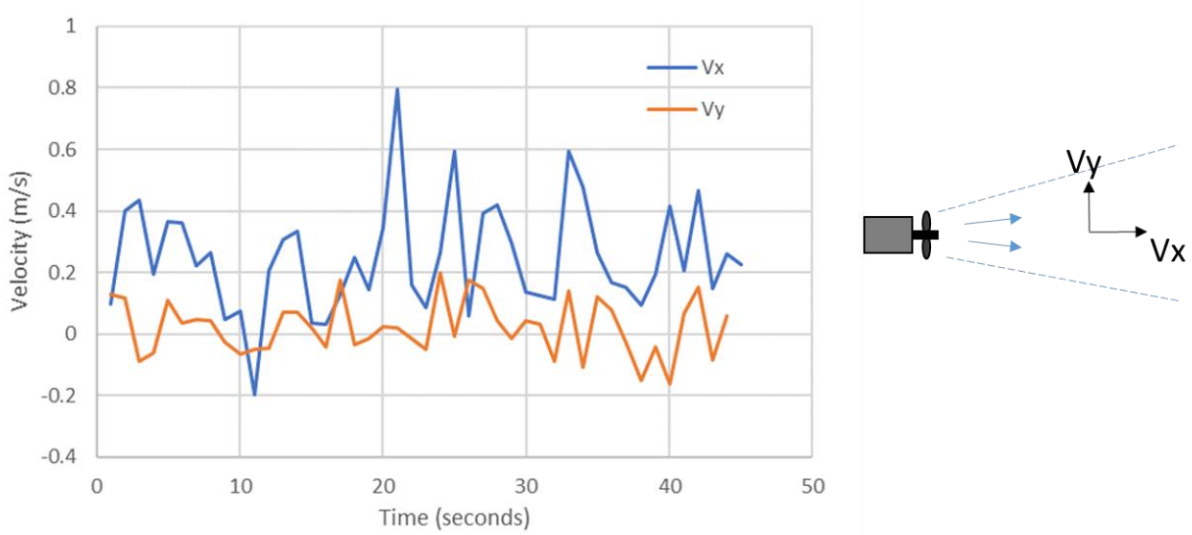

Figure 13: Example of 45-second velocity measurements at the public access boat ramp (Note 1 m/s = 3.28 ft/s). Vx is the velocity in the x-direction, approximately pointed towards the jet source, Vy is the lateral velocity, as shown above. The velocity magnitude is then $Vmag = \sqrt{V_x^2 + V_y^2}$.

Contour plots of velocities at the two ramps are given in Figure 14 and Figure 15, for velocities measured at 6-inch depth and mid-depth. The contours are somewhat irregular in shape at both sites, due to variations in water depth. The plots are orientated to give the approximate jet orientation to be along the x-axis (x and y are not orientated East-West and North-South). At the public ramp, the jet centerline bends south as the jet approaches the shoreline. At the Sheriff's ramp, the velocity increases at around 66 ft (20 m) distance from the jet as the flow passes over the concrete boat ramp.

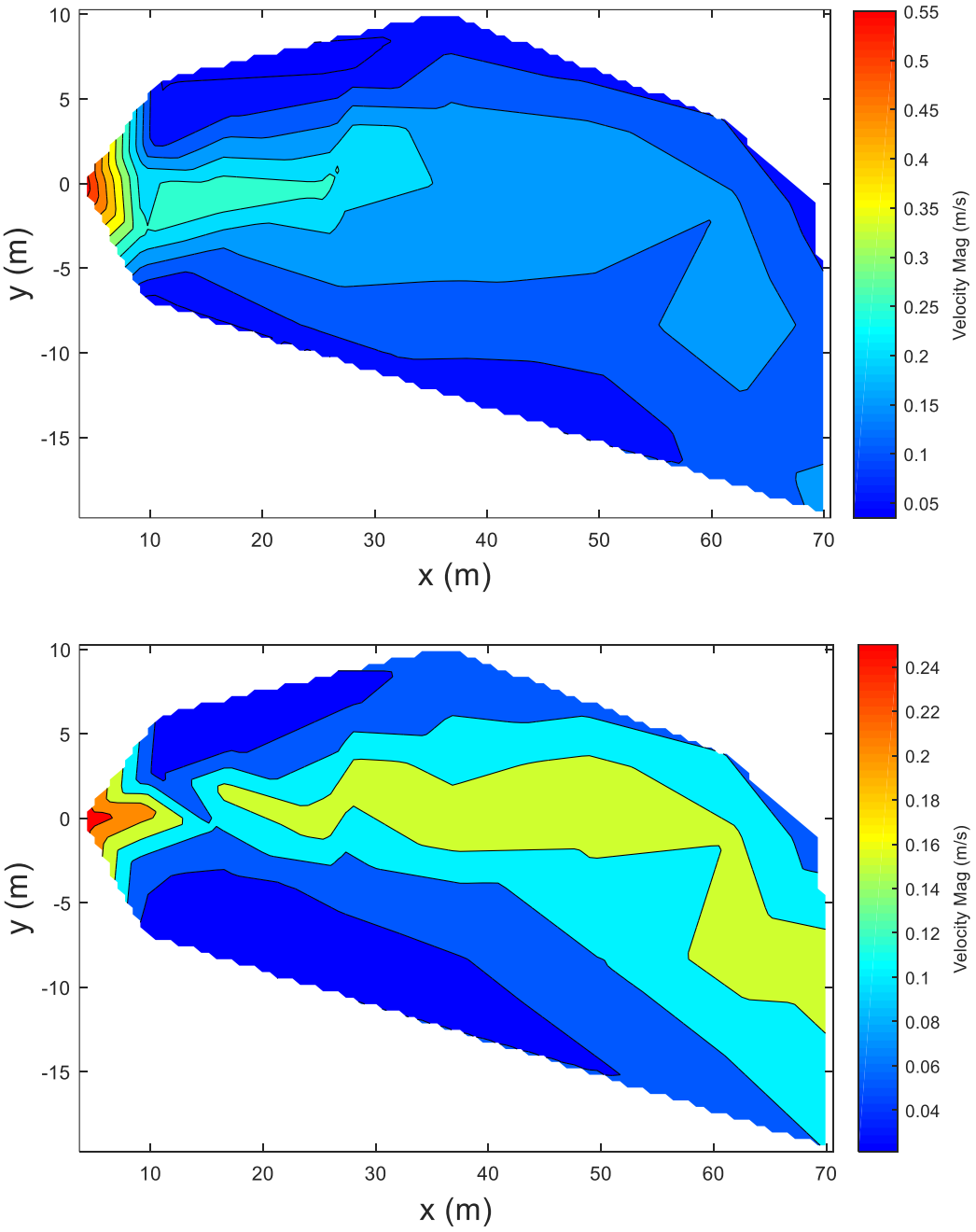

Figure 14: Velocity magnitude contours at the public boat ramp for measurements 6 inches below water surface (upper panel) and mid-depth (lower panel). Note: 10m = 32.8ft; 70m = 230ft; 0.2 m/s = 0.66 ft/s

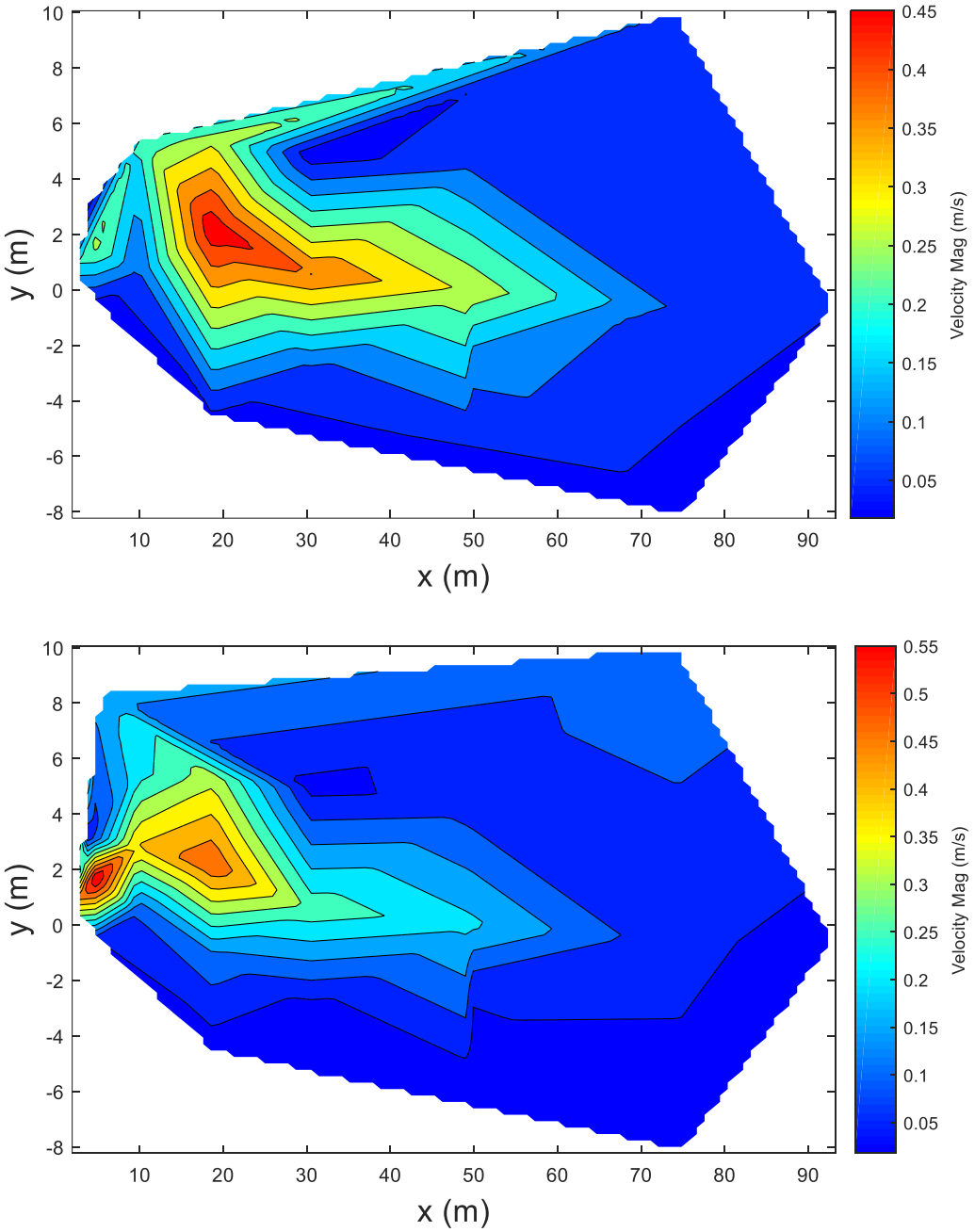

Figure 15: Velocity magnitude contours at the Sheriff's boat ramp for measurements 6 inches below water surface (upper panel) and mid-depth (lower panel). Note: 10m = 32.8ft; 90m = 295ft; 0.5 m/s = 1.64 ft/s

Figure 16 gives scatter plots of all velocity measurements versus distance from the jet source. At each distance, velocity varies depending on the depth of the measurement and on lateral distance from the jet centerline. The decay of maximum velocity with distance from the jet (r) at the public ramp ($Vmax=1.0*r^{-0.42}$) is similar to the decay rates seen in the idealized CFD models (e.g. Figure 33), while decay of maximum velocity with distance at the Sheriff's ramp is somewhat different ((Vmax=0.75*exp(-0.021*r)). A velocity of approximately 0.5 ft/s (0.15 m/s) was measured at 260 ft (80 m) distance at both sites, which suggests the jet's influence extends for over 250 ft along the centerline. The differences in

decay rate may be due to variations in the water depth, differences in the mounting angle of the jets with respect to horizontal, and the presence of aquatic plants. With the jets turned off, the average velocity magnitudes in the boat ramp areas were about 0.06 ft/s (0.02 m/s) at both sites, suggesting that the jet units still produce measurable velocities 260 (80 m) from the source.

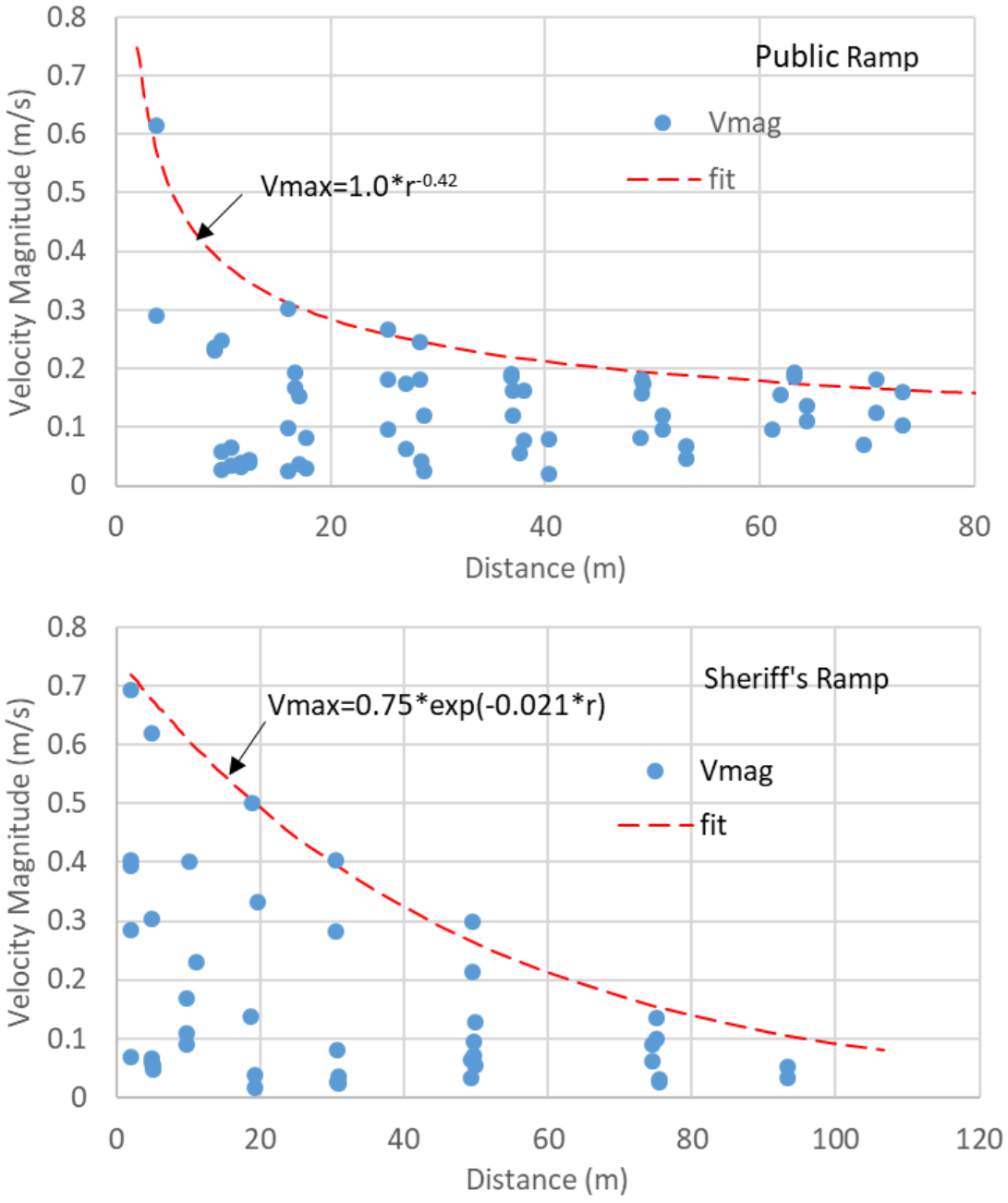

Figure 16: Scatter plot of all measured velocity magnitudes vs. distance from jet source for the public ramp (upper panel) and the Sheriff's ramp (lower panel). Also shown are fits to the maximum velocity magnitude vs. distance (r). Note 1 m/s = 3.28 ft/s; 80m = 260ft

4 Conclusions and Recommendation

In general, most (67%) observations showed less mass of suspended vegetation fragments with the jet operating compared to the mass of suspended vegetation fragments before the jet was turned on. **In other words, submersed jets reduced the amount of suspended plant fragments when used near boat ramps.**

Some samples (33%) produced more plant fragments with the jet on, and these may be explained by mobilization of suspended plant fragments near the jet when it was turned on, increasing transport of the plant fragments towards the jet. There are at least three recommendations to overcome this challenge: 1) the jet should be placed away from areas where plant fragments will accumulate in abundance, 2) plant fragment accumulation should be prevented around and near the jet, or 3) accumulated plant fragments should be prevented from being pulled in by the submersed jets.

In some tests, the amount of suspended plant fragments after the jet was turned off was less than before the jet was turned on, indicating that the jet provided a positive effect for some time after operation. This post-operation effect was not measured, but visual observations suggested the benefit would last until natural wind-driven transport of suspended plant fragments pushed fragments back into the area of the jet's influent.

Field ADV measurements confirmed computer simulations that submersed jets can impact surface velocity by up to 250 ft away from the jet and overcome a typical drift velocity of 0.66 ft/s to push suspended plant fragments away from boat ramps. High winds or winds opposite of the jet and dense submerged rooted vegetation will reduce these distances. Also, the horsepower (hp) of the jet installed in the field was 0.5 hp. While jets with more horsepower (hp) produce greater jet velocities, the relationship is not linear nor 1:1. For example, a 0.75 hp jet will produce jet velocities that are ~50% greater than a 0.25 hp jet (e.g., see Figure 17, Supplemental Information). Because submersed jets have the potential to impact distances of 200 ft or more, it's important to consider the banks, shore, and structures along the centerline of the jet to ensure 1) plant fragments pushed by the jet have an appropriate destination, and 2) erosion and damage by the jet is prevented.

Jet positioning is important for efficiently and effectively moving suspended plant fragments. Computational Fluid Dynamics (CFD) simulations for simple geometries (see Supplemental Information, Section 6.1.5) were used to determine the effect of motor angle on the jet velocity and bottom shear stress. In the vertical direction, the jet should be placed at least 20 inches above the lake bottom and with a vertical angle that is greater than 10° above level (towards the water surface) to minimize scour of fine sediment. The jet can be positioned with angles above level ranging to 20° or larger, but the longest distance of impact is achieved with the shallowest angle (e.g., 10°).

In the horizontal direction, the jet should be placed facing parallel to the shore or towards the shore such that suspended plant fragments are pushed across or away from the boat ramp. Positioning the jet such that the centerline points away from the boat ramp may create a recirculation zone on the bottom ramp (e.g., observed at Weaver Lake), where suspended plant fragments can accumulate and exacerbate the potential for plant fragment trapping on boat trailers. Additional research is warranted to understand the full extent of submersed jets on minimizing spread of aquatic invasive species, the feasibility and practicality of solar-powered stations, and additional validation of modeling results to field measured data.

5 Drone data availability

Drone photos and videos were collected as part of this project. This photographic and videographic data was shared with Hennepin County Staff when this final report was submitted and is the property of Hennepin County.

6 Supplemental Information – Verification of Simulations

6.1 Computer Simulations & Lab Verification

Not all conditions can be measured in the field, but computer simulations can replicate simplified conditions and many variations of jet position, flow velocity, and other factors that affect the efficiency of submersed jets. First, the computer simulations were verified to ensure the computer simulations accurately represent real velocities produced by the jet.

6.1.1 Estimating jet velocities

The exit velocity of a submerged jet produced by a propeller (V_o) can be estimated based on the propeller diameter and the motor horsepower using the following equation (Symonds et al. 2016):

$$V_o = 1.15 \left(\frac{P}{\rho D_o^2}\right)^{1/3} \quad (1)$$

Where P is power, ρ is the density of water, and D_o is the propeller diameter. For a 7-inch (18 cm) diameter propeller and a ¾ horsepower motor, the estimated jet velocity is 3 m/s (9.8 ft/s). The variation of V_o with motor power is illustrated in Figure 17. For a ½ horsepower motor, the estimated jet velocity is 2.6 m/s (8.6 ft/s). As demonstrated by Figure 17, increasing horsepower does not linearly increase jet velocity (i.e., buying stronger jets may not be more cost-effective).

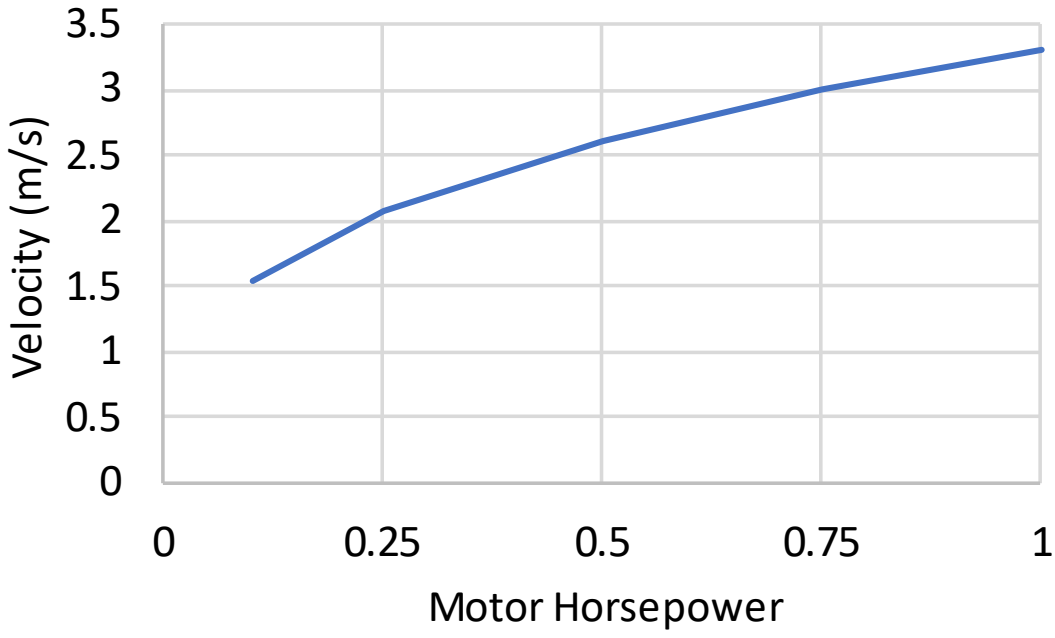

Figure 17: Propeller exit velocity vs. motor horsepower for a 7 in. diameter propeller, based on Equation 1.

For a submerged jet in a large body of water, the decay of velocity with distance and the width of the jet can be estimated with the following equation (Symonds et al. 2016):

$$V(x,r) = 2.8\, V_o \left(\frac{D_o}{x}\right) exp\left[-15.4\left(\frac{r}{x}\right)^2\right] \quad (2)$$

where x is the distance from the jet source along the jet centerline, r is the radial distance from the jet centerline, and D_o is the jet diameter (Figure 18). The corresponding decay of velocity for the ¾ horsepower jet is shown in Figure 19, along with the width of the jet with distance. Equation 2 only applies outside of a minimum distance from the jet source, about 3 times the propeller diameter. As the jet travels through the water, it expands by entraining ambient fluid from the sides via turbulent eddies and slows down, because the jet loses momentum as the ambient water is entrained.

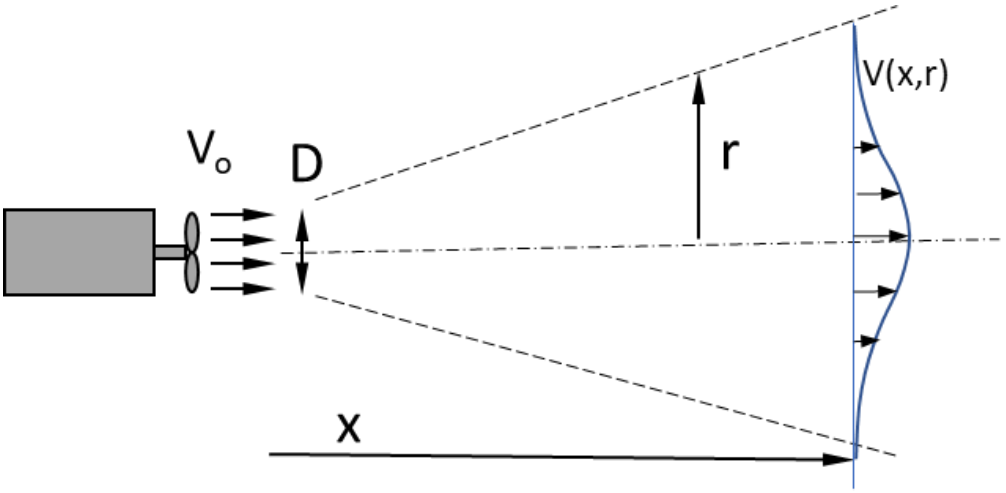

Figure 18: Schematic diagram of a submerged jet produced by a motor and propeller.

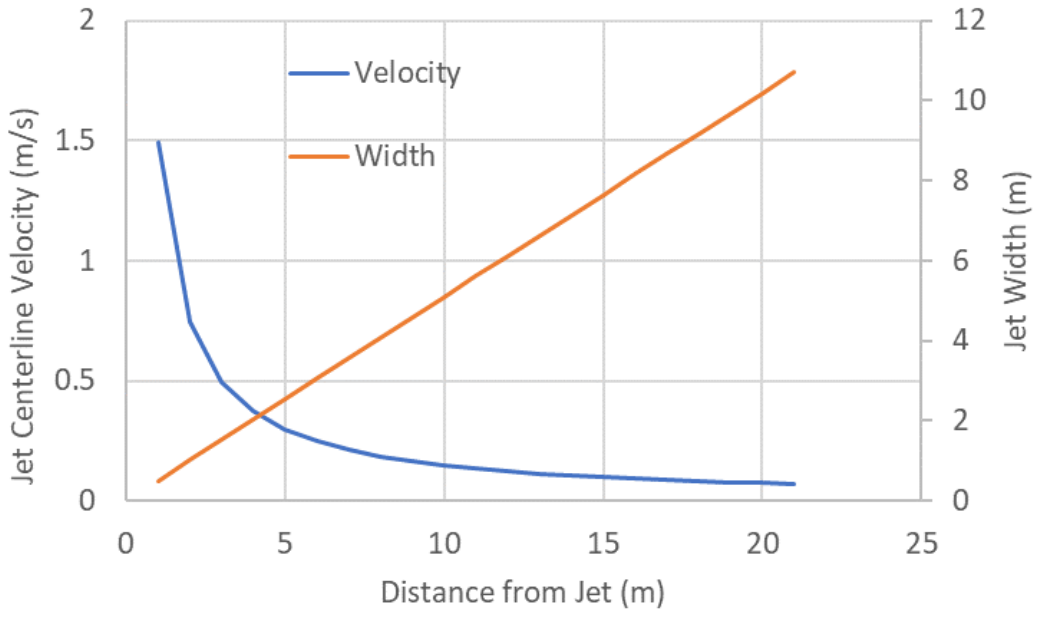

Figure 19: Estimated jet centerline velocity and jet diameter over distance, from Equation 2. The width is based on the distance from the jet centerline where the velocity is 37% of the centerline velocity.

For a submerged jet in a shallow area of a lake, the expansion of the jet with distance is constrained by the water surface and the lake bottom. Both of these boundaries reduce the decay rate of the jet, because the boundaries limit the amount of fluid that can be entrained (Raiford and Khan 2009, Chowdhury et al. 2017). Plane jets at the water surface (surface jets) have been shown to decay with distance (x) as $x^{-1/2}$, compared to x^{-1} for circular free jets (Rajaratnam and Humphries, 1984). The bottom boundary does give some resistance to the fluid motion and loss of momentum, but generally less than the momentum loss due to fluid entrainment in a very deep domain. As a result, the submerged jet decay rates observed in typical lake installations should be lower than those predicted by Equation 2, unless there is substantial submerged or emergent plant cover. This is demonstrated in Section 6.1.3 using computational fluid dynamics models.

6.1.2 Laboratory testing of an Aqua Thruster

To help verify the simple submerged jet models given above and the more complex computation fluid dynamics models described later, a ¾ hp Aqua Thruster unit was installed in the St. Anthony Falls Lab main channel, which is 275 ft long, 9 ft wide, with a maximum depth of 5.9 ft. Note that because the channel is only 9 ft wide, the jet velocity distribution that was measured in the channel is not the same as it would be in a lake, because the water recirculates back to the jet source along the sides and bottom of the channel, creating additional momentum loss for the jet. The main purposes of the experimental test were to 1) verify the outlet velocity of the jet (Eq. 1) and 2) verify that the computational fluid dynamics (CFD) model was able to reproduce the jet velocity distribution in the channel.

The Aqua Thruster was placed on the channel bottom approximately 20 m from the upstream end of the channel (Figure 20 & Figure 21). The motor mount frame was adjusted such that the motor/propeller were pointed upwards 15° from horizontal, and center of the propeller was 0.56 m (22 in.) above the channel bottom, which was covered with coarse sand. The channel was filled with river water, with a depth of 1.06 m (42 in.). A Vectrino ADV (Acoustic Doppler Velocimeter) mounted to the instrument cart was used to take a series of velocity measurements at different locations in the channel, starting 1 m from the propeller hub. At each location, velocity data was taken at 100 Hz for 90 seconds and stored in a file. The velocity data was filtered to remove noise spikes, and the mean and fluctuating velocity components were calculated. An example of the measured velocity data is given in Figure 22, with more measured data given in Section 6.1.4 in comparison to CFD modeled results.

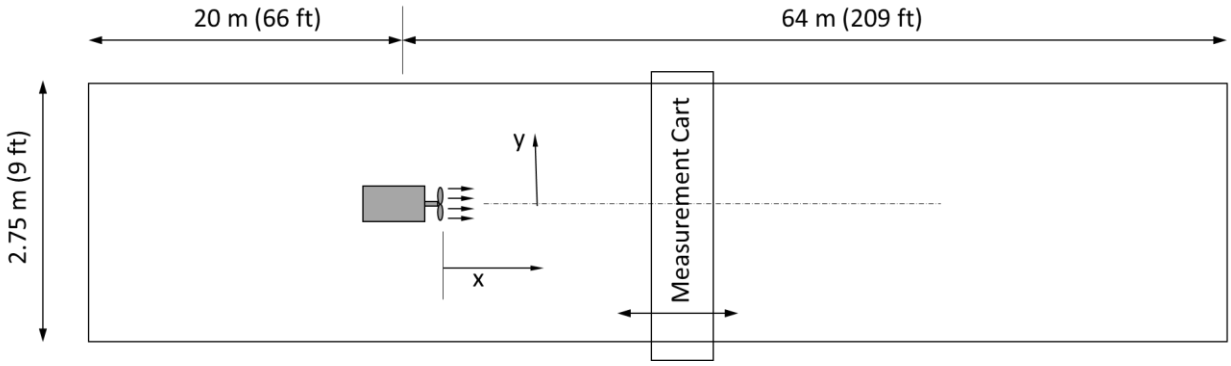

Figure 20: Map view of the experimental setup of the Aqua Thruster in the SAFL main channel (not to scale).

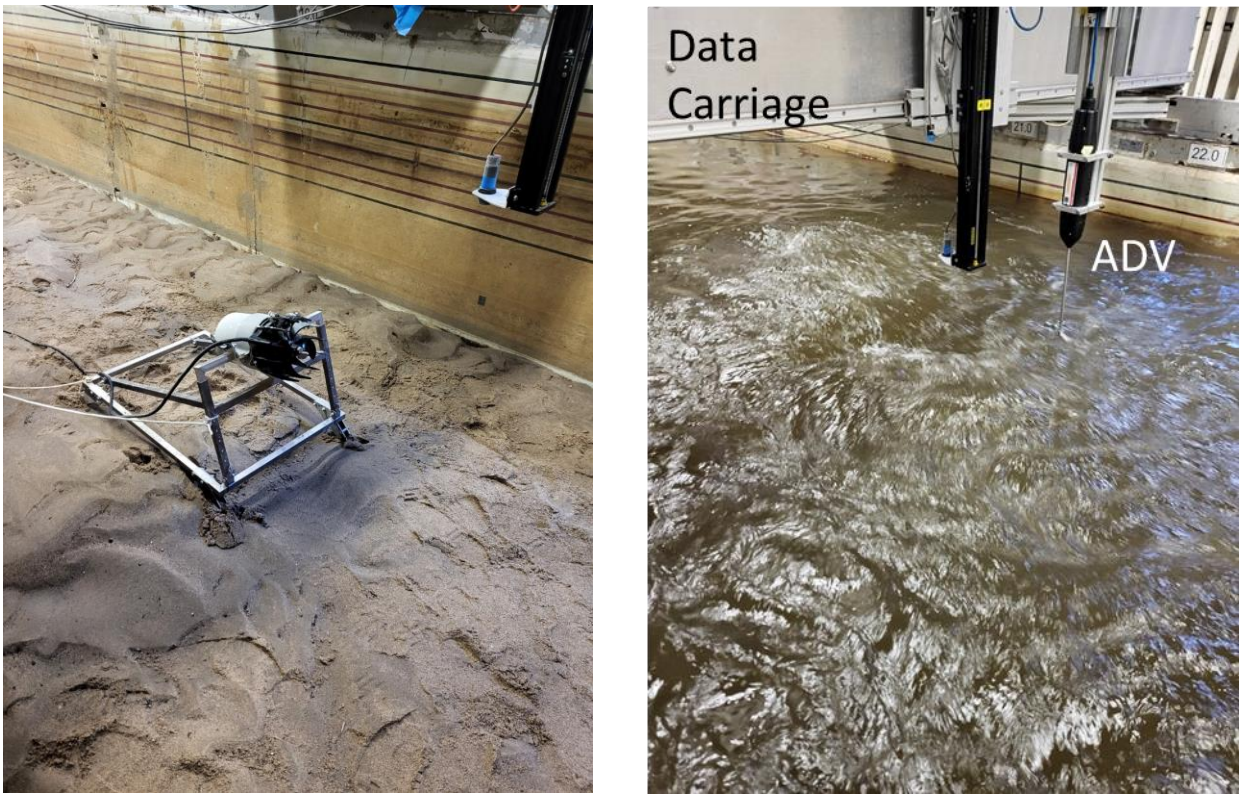

Figure 21: Photographs of the Aqua Thruster installed in the SAFL main channel (left) and the surface jet produced by the Aqua Thruster and the ADV used to measure velocities suspended from the data carriage (right).

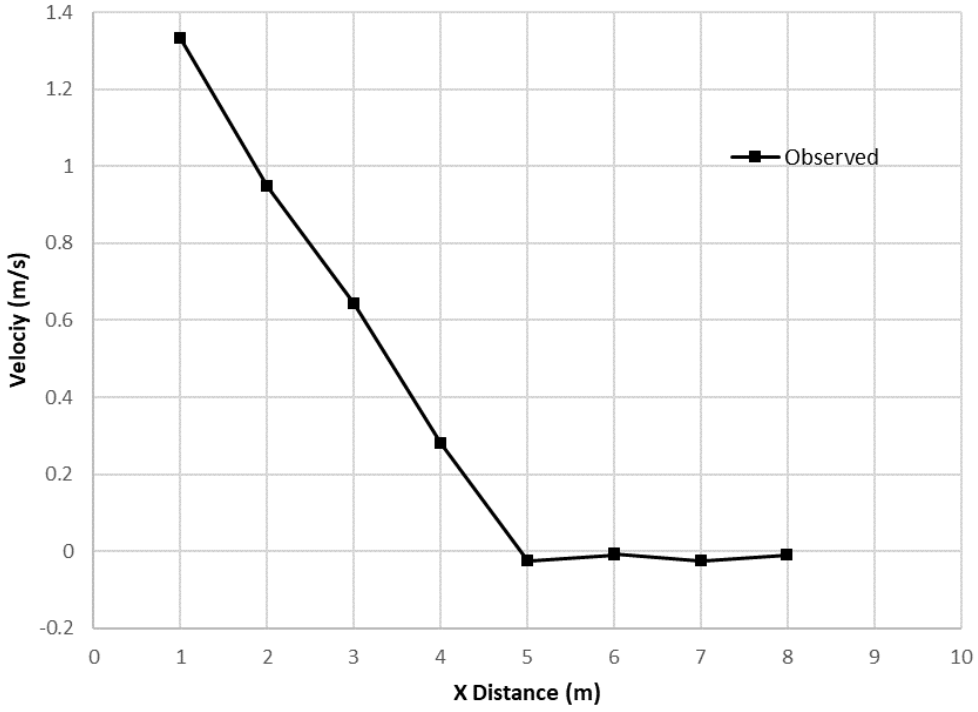

Figure 22: Velocity magnitude vs. distance (x-direction) along the channel center (y=0) and at a depth of 10 cm (3.9 in).

6.1.3 CFD Models for Turbulent Jets in Deep and Shallow Water

A simple, rectangular domain computational fluid dynamics (CFD) model was assembled to investigate the ability of CFD to simulation turbulent jet decay in deep and shallow water (see Figure 23). To model a free jet in deep water, the modeling domain was 40 m wide and thick, and 100 m long, with a 15 cm diameter jet with an inlet velocity of 4 m/s. To model jets in shallow water, the thickness was reduced to 10 m and to 2 m, keeping the width at 40 m. A shallow water case with a free surface was also modeled using a frictionless surface for the top.

The velocity decay rate from the CFD model results matches the slope of the free jet model (Eq. 2) for either 10 m or 40 m thick domains (Figure 24). For the 40 m wide x 2 m thick model, the jet velocity transitions to a lower slope ($x^{-1/4}$) at about 10 m from the jet source. This low decay rate is even lower than that of a surface jet ($x^{-1/2}$) and represents the combined effects of constraints by the surface and bottom. In this case, the results were similar for the 2 m thick domain for a free surface or fixed (no slip) surface (Figure 25).

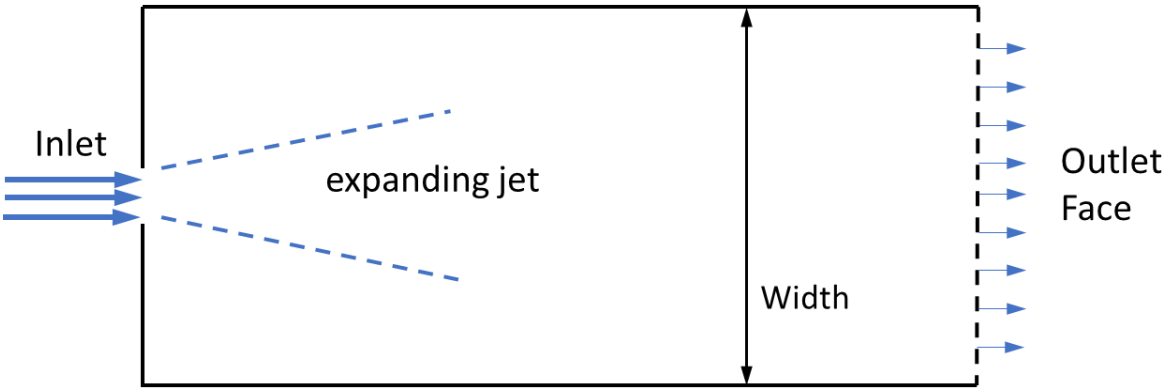

Figure 23: Schematic of the CFD model domain for modeling the decay of a turbulent round jet.

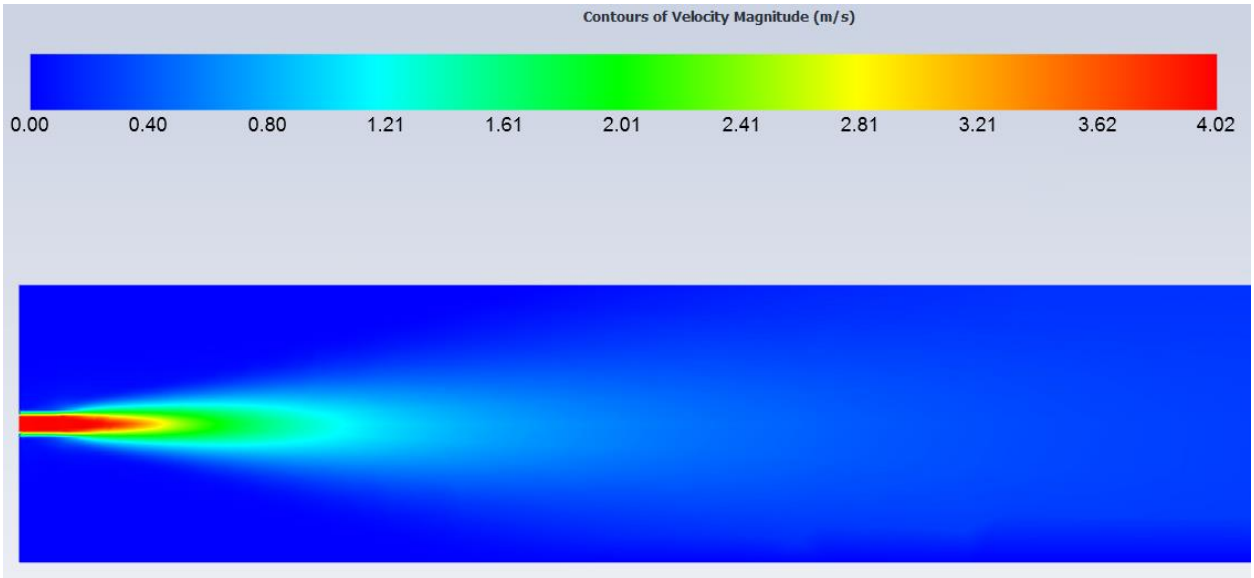

Figure 24: Plot of modeled velocity magnitude along the domain centerline, near the jet source, for the 2 m thick domain and a 15 cm diameter jet at the inlet.

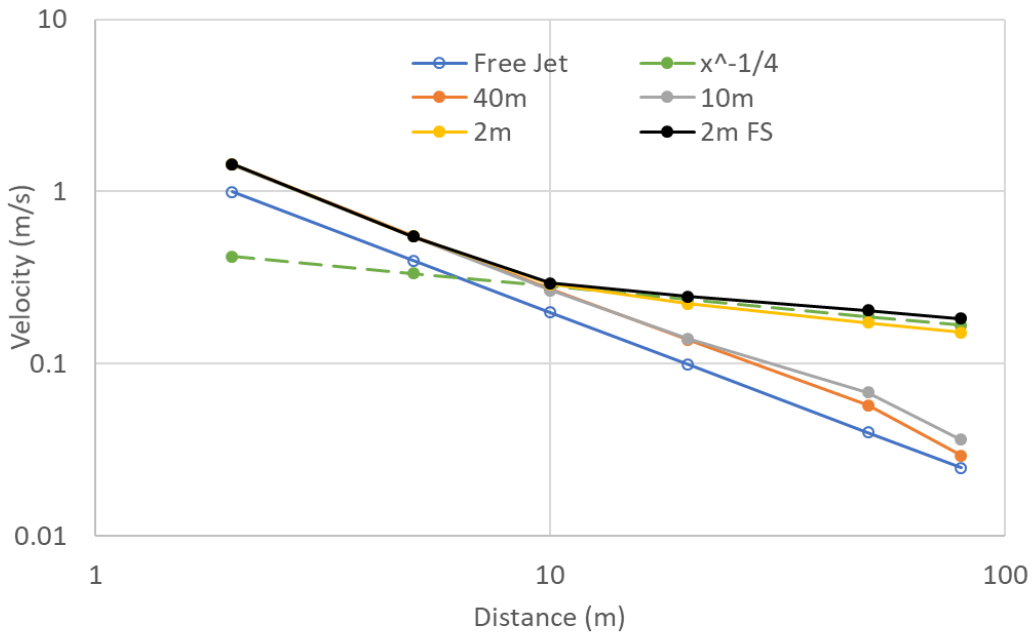

Figure 25: Simulated decay rate of centerline jet velocity for 40 m, 10 m, and 2 m thick domains, along with the free jet solution (Eq. 2) and a line with slope $x^{-1/4}$. 2 m FS has a frictionless surface on the top of the domain.

6.1.4 CFD model for the Aqua Thruster in the SAFL Main Channel

A CFD model for the Aqua Thruster in the main channel was created in Ansys-Fluent. Assuming the velocities are symmetrical about y=0 (Figure 18), one half of the main channel was modeled. The Aqua Thruster was represented in the CFD model by a disk-shaped fixed velocity source and a second disk-shaped fixed wall to represent the motor face (Figure 26), such that flow into the disk (propeller) is obligated to come in radially from the sides. The upper water surface was represented as a wall with zero shear stress. The CFD model had about 290,00 nodes to represent ½ of the main channel. The k-ε turbulence closure scheme was used with the default coupled solver in Ansys-Fluent.

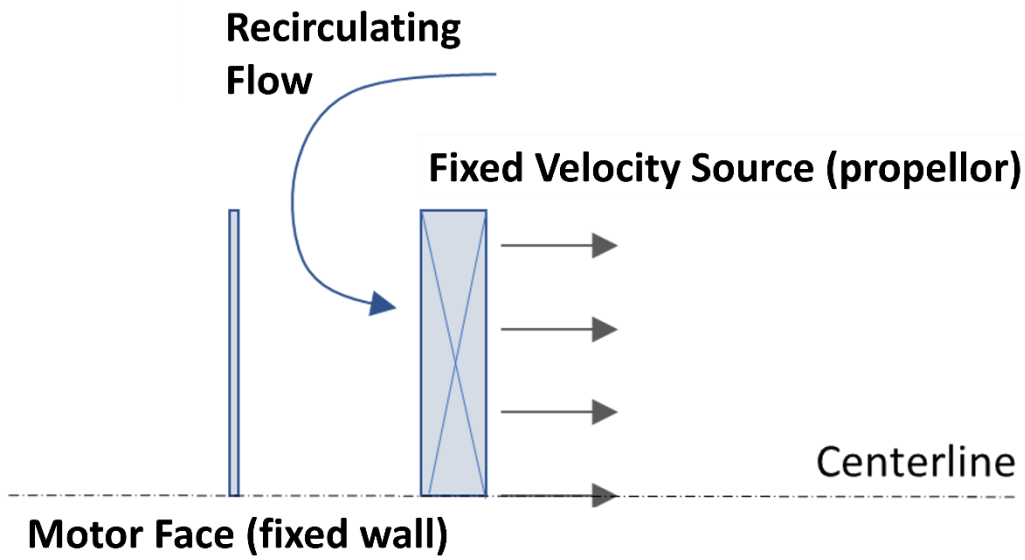

Figure 26: Detail schematic of the representation of the Aqua Thruster in the CFD model.

Contour plots of velocity for typical CFD simulations showing velocities on a vertical slice down the center line of the channel (Figure 27) and the velocities at the water surface from the centerline to the edge of the channel (Figure 28) show the area of effect provided by the jet. The model was run for a series of motor angles (10°, 15°, 20° and 25°) from horizontal (0°). Plots of the simulated near-surface velocity along with the measured velocities from the test suggest that although the motor was set to a 15° angle, it may have shifted in the sand bed when it was turned on to an angle closer to 20° (Figure 29). Figure 29 also suggests that a longer surface jet may be obtained by setting the motor at a shallower angle (closer to horizontal). Velocity plots along two lateral transects (Figure 30) and a vertical transect near the Aqua Thruster (Figure 31) show good agreement between the CFD simulations and the measured velocities.

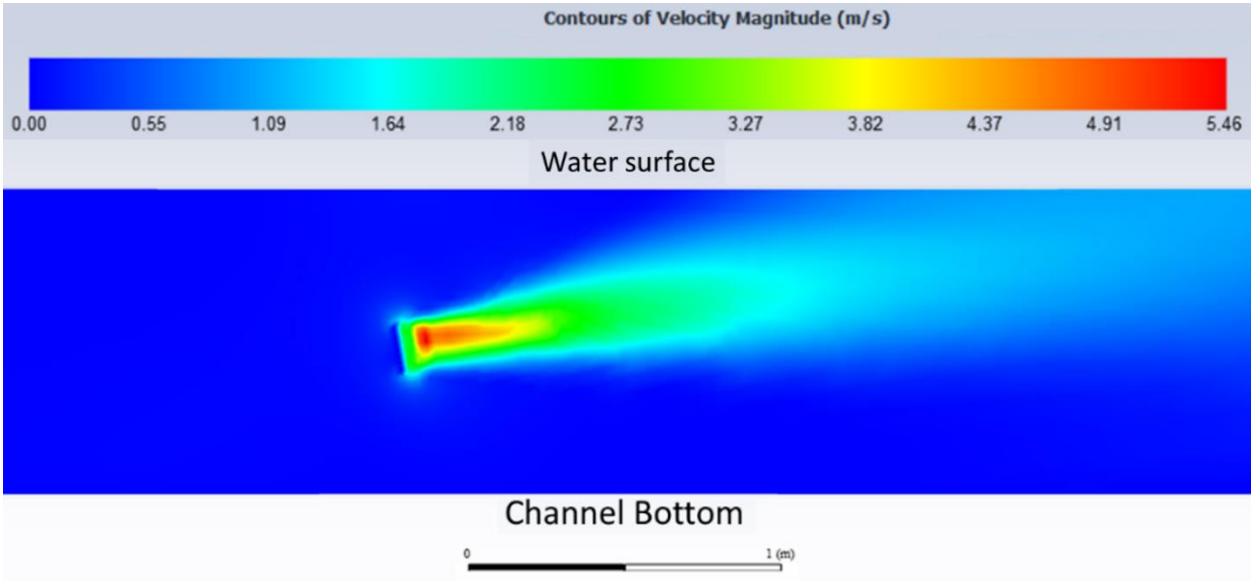

Figure 27: Plot of modeled velocity magnitude near the Aqua Thruster along the channel and jet center line (y=0) for the motor set at a 10° angle from horizontal.

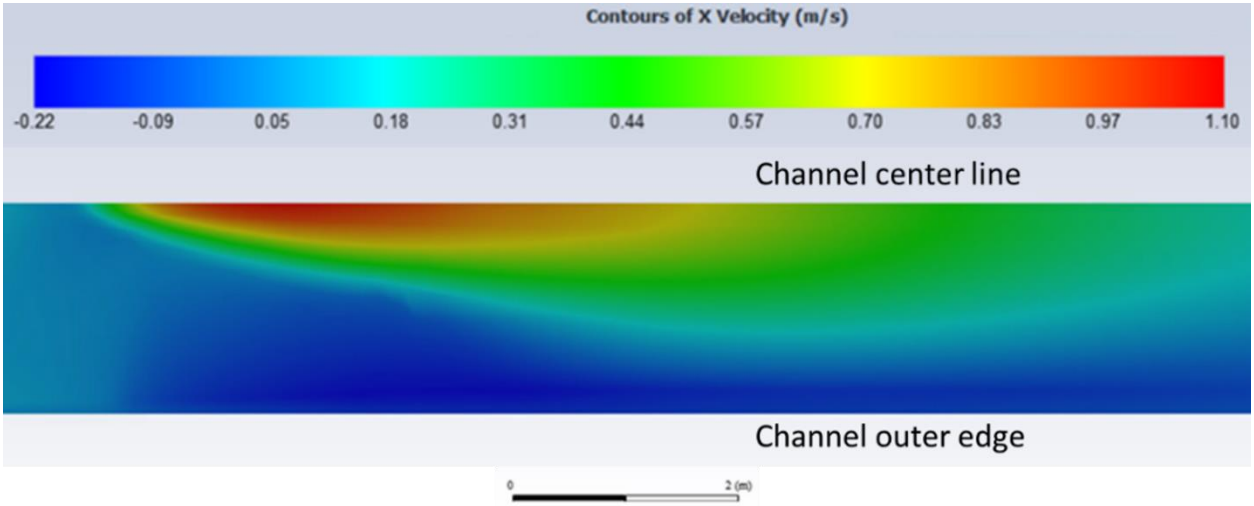

Figure 28: Plot of modeled velocity (x-component) near the Aqua Thruster at the water surface for the motor set at a 10° angle from horizontal. Note that the velocity is negative near the edges due to recirculating flow.

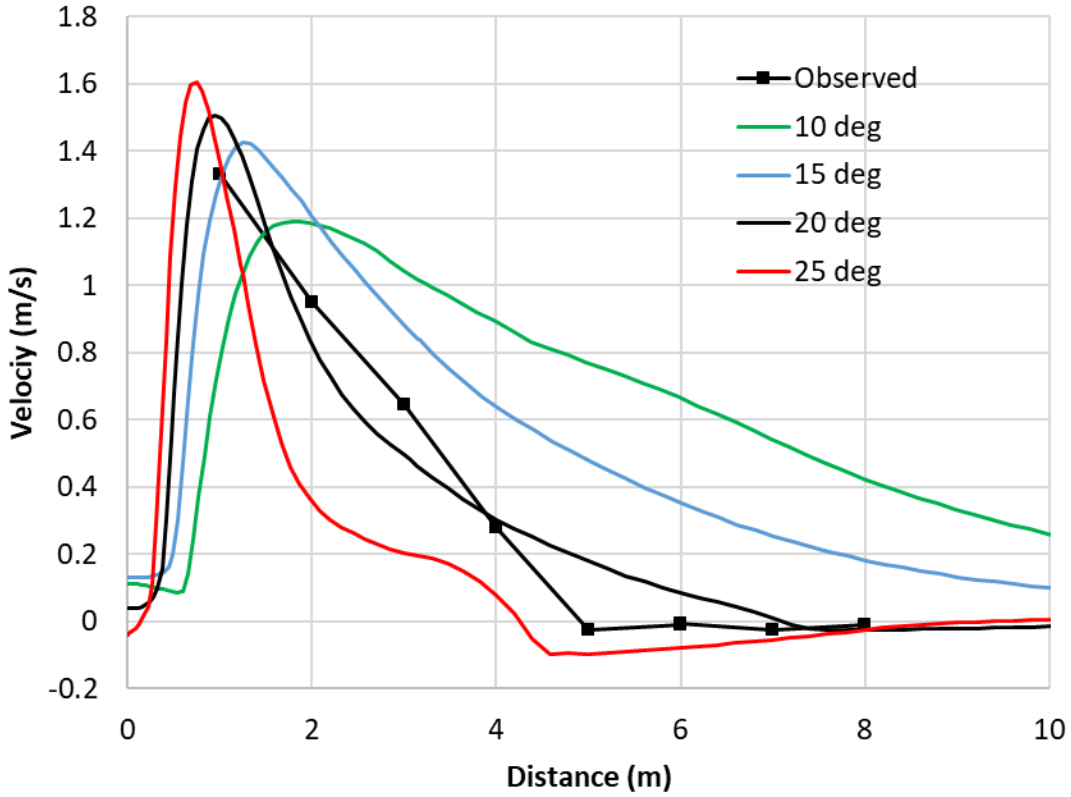

Figure 29: Plot of observed and modeled (CFD) velocity magnitude vs. distance (x-direction) along the jet center line. Modeled velocities are given for 4 different motor angles from horizontal.

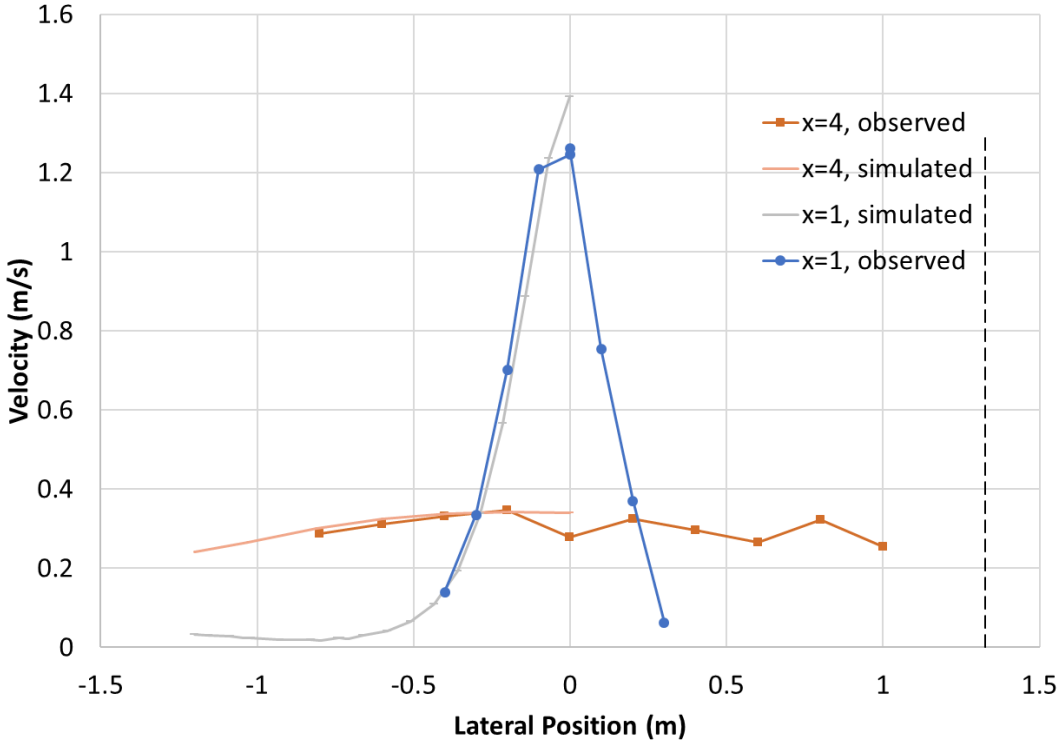

Figure 30: Plot of observed and modeled (CFD) velocity magnitude vs. lateral distance (y-direction) at 1 m and 4 m downstream from the Aqua Thruster. Modeled velocities are given for a 20° angle from horizontal.

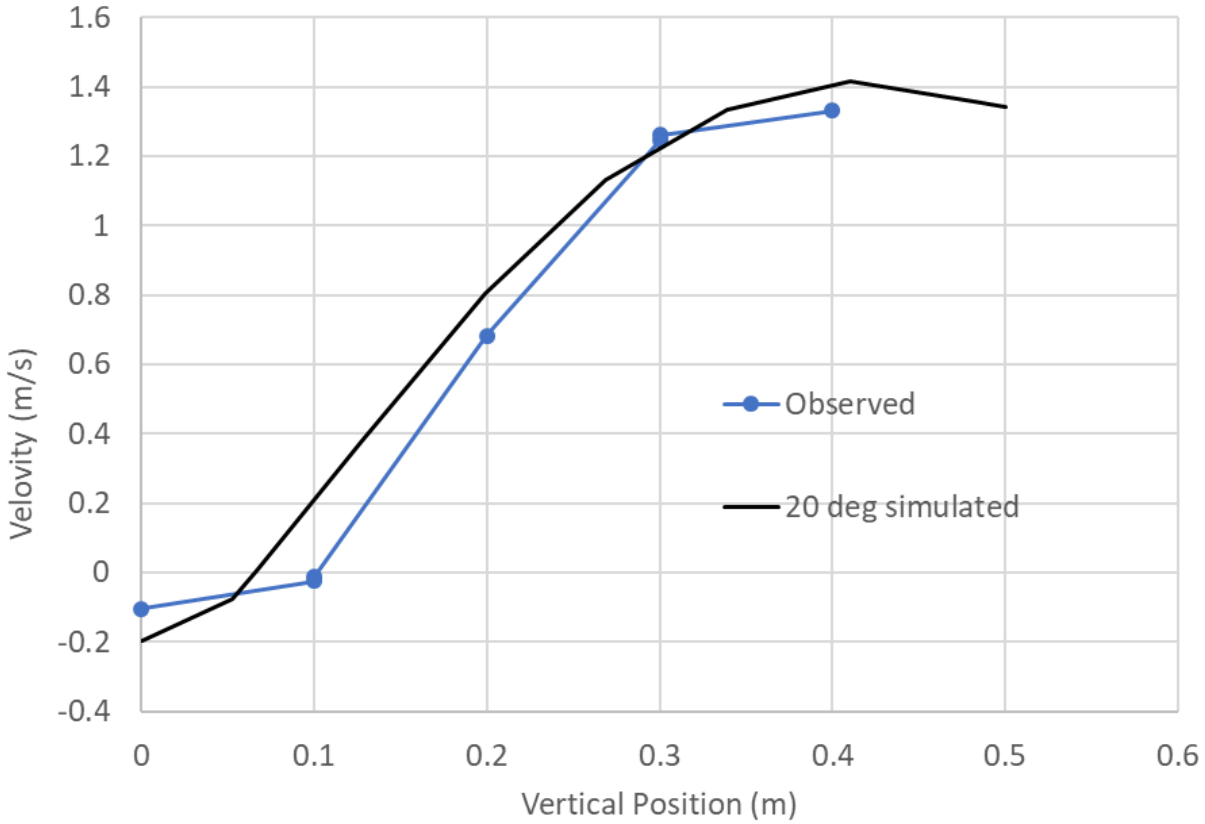

Figure 31: Plot of observed and modeled (CFD) velocity magnitude vs. vertical distance (z-direction) at 1 m downstream from the Aqua Thruster. Modeled velocities are given for the motor at a 20° angle from horizontal.

6.1.5 CFD model for the Aqua Thruster in a wide channel

The measurements of CFD simulations of the Aqua Thruster in the SAFL main channel suggest that the length of the jet plume (and the effective distance for clearing debris) may depend on the mounting angle from horizontal. To explore this behavior further, and to also explore the possibility for bottom scour, another set of CFD simulations was made using a much wider channel (40 m wide) to reduce the impact of recirculating flows and better approximate a lake installation. Rather than modeling a closed-end channel, like the SAFL main channel, an open-ended model was used, similar to the CFD model in Section 6.1.3 (Figure 23), to further reduce the amount of recirculation back the jet source. Variations in the motor mounting angle were modeled by varying the vertical and horizontal velocity components at the source. The simulation domain was 40 m wide x 1 m deep x 60 m long, with a jet source diameter of 0.178 m and a velocity magnitude of 3 m/s, centered 0.56 m from the bottom. The angle of the motor from horizontal was varied from 0° to 20°. As with previous models, ½ of the domain was simulated, assuming symmetry around the channel centerline.

Typical simulation results for the surface velocity and bottom shear stress for a 15° motor angle are given in Figure 32. As the jet expands from x=0, it reaches the surface and the channel bottom. The surface velocity along the channel centerline does vary with the motor angle (Figure 33), with higher angles producing larger velocities closer to the jet source and decreasing faster with distance. Increasing the depth of the channel to 2 m substantially reduced surface velocities, due to more initial entrainment before getting to the surface and a longer surface jet region.

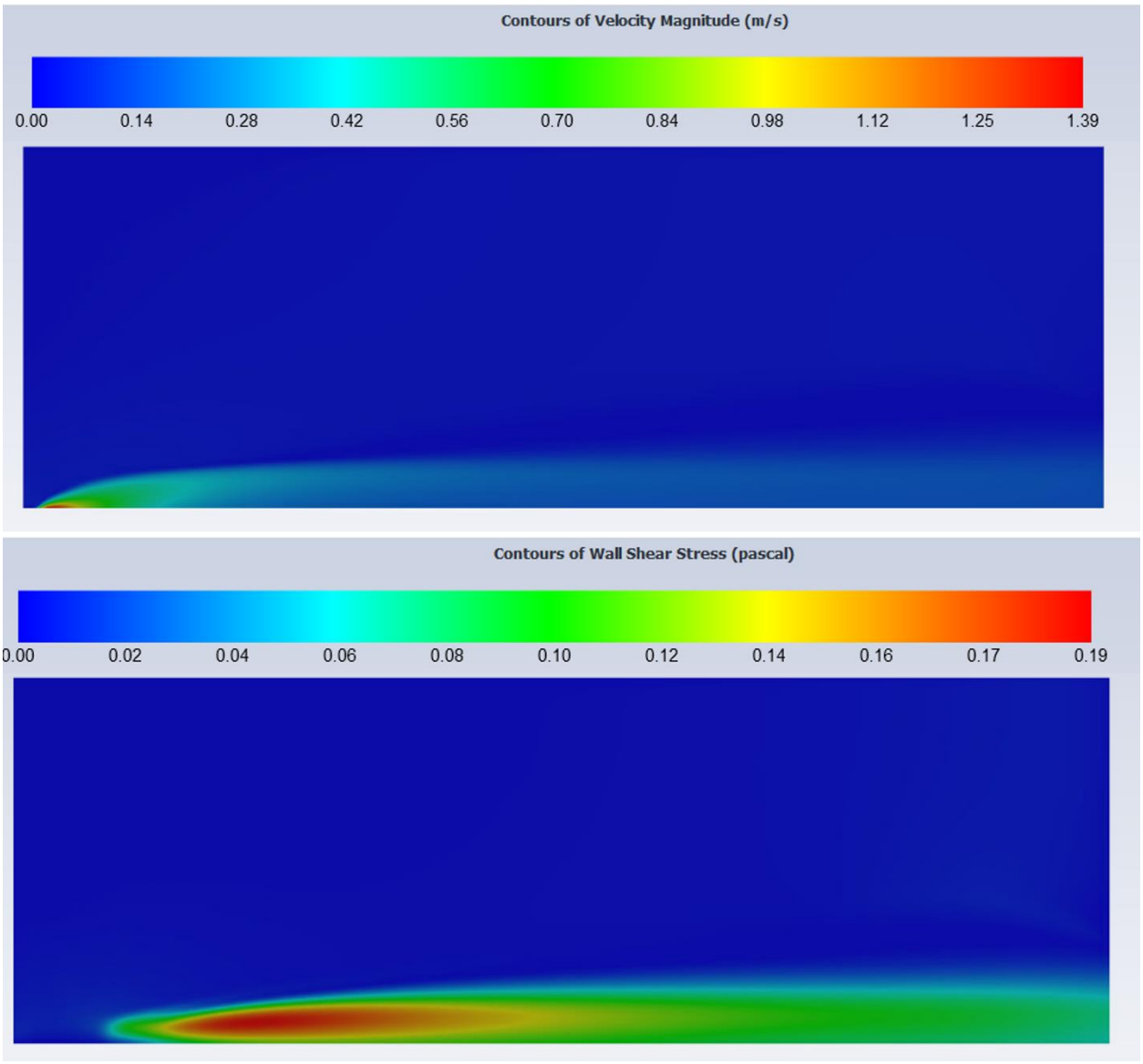

Figure 32: Contour plots of surface velocity magnitude (upper panel) and bottom shear stress (lower panel) for the motor at a 15° angle from horizontal.

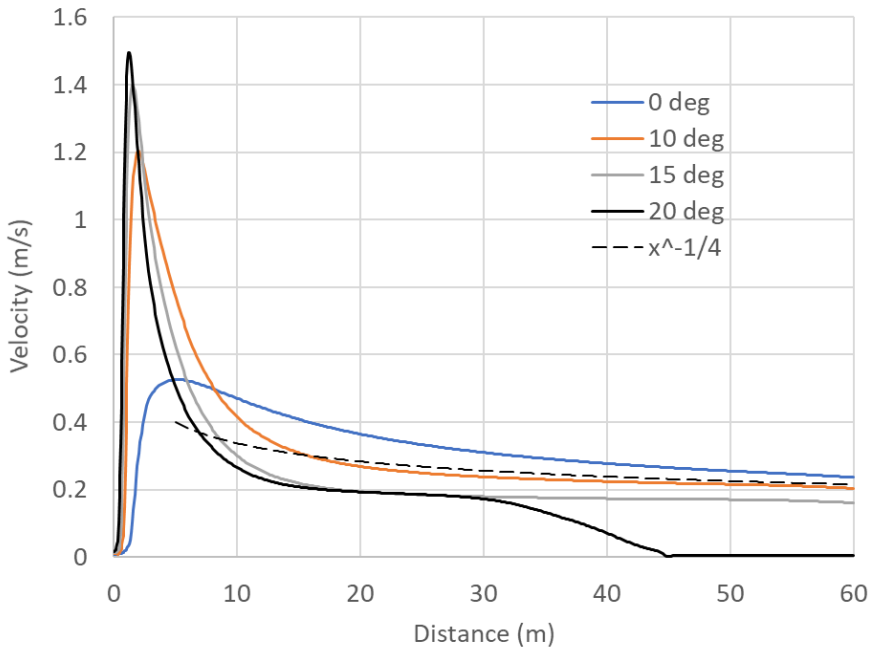

Figure 33: Velocity vs. distance at the water surface above the jet centerline for motor angles of 9°, 10°, 15°, and 20° from horizontal. A line that follows x^-1/4 is also given for reference.

The drift velocity on a lake surface is approximately 3% of the wind speed (Wu 1975) but may be lower in small lakes and sheltered bays. For a 15 mph (6.7 m/s), the estimated drift velocity is 0.2 m/s. For a jet to be effective at moving floating and suspended plant fragments, then the surface velocity due to the jet should exceed the drift velocity. In ideal conditions, a 10° motor angle produced surface velocities exceeding 0.2 m/s out to the 60 m domain length. In a lake, the surface velocity may decrease more quickly than the idealized case modeled, if the jet passes over deeper water or if obstructions such as docks and submersed plants are in the path.

The simulated maximum bottom shear stress was recorded for each motor angle and found to be nearly constant (0.2 Pa) for motor angles of 10° or greater but increased for shallower angles (Figure 34). For reference, the shear stress required to resuspend sediment varies with grain size (Wilcock 1993), but 0.2 Pa is the approximate critical shear stress for 0.3 mm diameter sediment (fine sand). Figure 35 illustrates that motor angles of 0° – 5° produce substantially greater shear stress and would likely mobilize (i.e., scour) fine sand particles, whereas motor angles of 10° or greater are unlikely to mobilize fine sand particles.

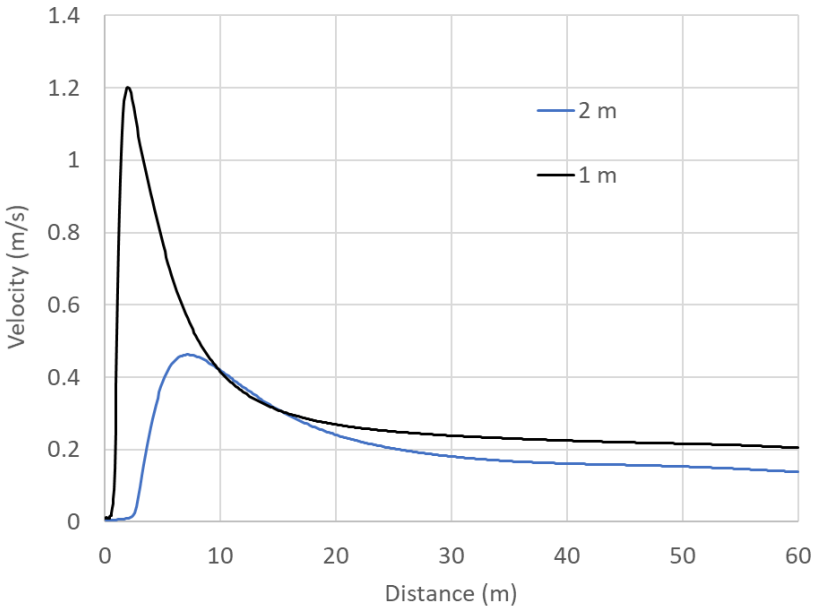

Figure 34: Velocity vs. distance at the water surface above the jet centerline for 1 m and 2 m deep channels and a 10° motor angle.

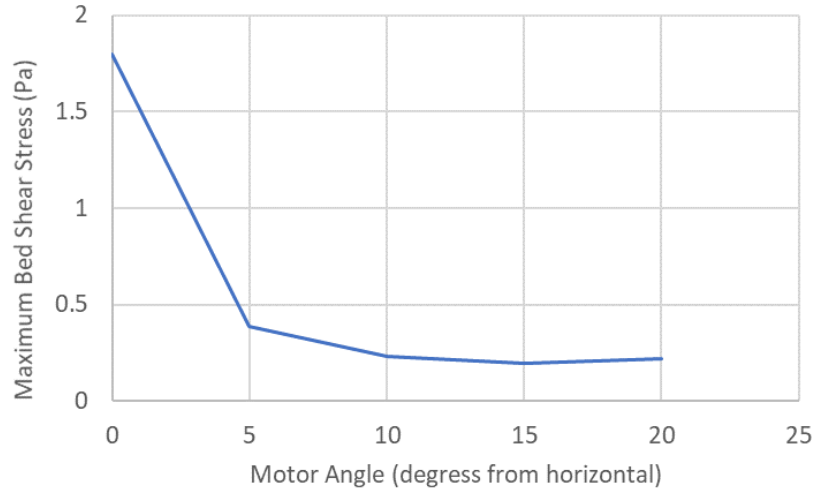

Figure 35: Simulated maximum bed shear stress vs. motor angle for a 1 m deep channel.

7 References

Chowdhury, M. N., Khan, A. A., & Testik, F. Y. (2017). Numerical investigation of circular turbulent jets in shallow water. Journal of Hydraulic Engineering, 143(9), 04017027.

Raiford, J. P., & Khan, A. A. (2009). Investigation of circular jets in shallow water. *Journal of hydraulic research*, *47*(5), 611-618.

Rajaratnam, N., & Humphries, J. A. (1984). Turbulent non-buoyant surface jets. journal of Hydraulic Research, 22(2), 103-115.

Riley, M.J. and Stefan, H.G. (1987). Dynamic Lake Water Quality Model, "MINLAKE". University of Minnesota St. Anthony Falls Project Report #263, 146 pp.

Symonds, A., Britton, G., Donald, J., & Loehr, H. (2016). Predicting propeller wash and bed disturbance by recreational vessels at marinas. In Bulletin of the Permanent International Association of Navigation Congress PIANC (pp. 70-80).

Wilcock, P. R. (1993). Critical shear stress of natural sediments. Journal of Hydraulic Engineering, 119(4), 491-505.

Wu, J. (1975). Wind-induced drift currents. Journal of Fluid Mechanics, 68(1), 49-70.